ChemPubSoc Europe
DOI: 10.1002/cssc.201901880
CHEMSUSCHEM Reviews

Biomass-Derived Carbon: A Value-Added Journey Towards Constructing High-Energy Supercapacitors in an Asymmetric Fashion

M. L. Divya,[a] Subramanian Natarajan,[a] Yun-Sung Lee,*[b] and Vanchiappan Aravindan*[a]

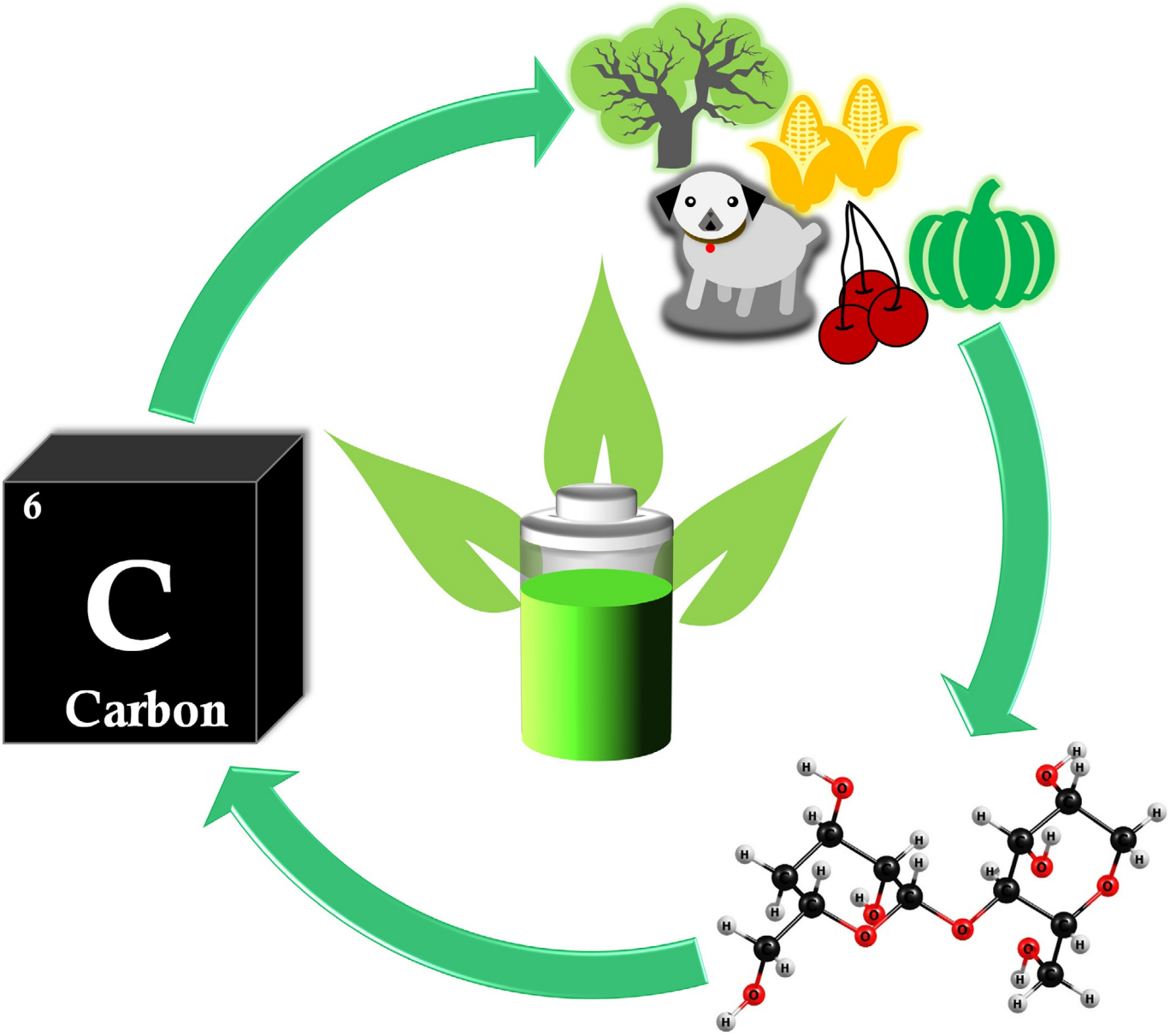

Currently, asymmetric supercapacitors (ASCs) produced from supercapacitors (SCs) offer more benefits for energy-storage applications because they display a high operational voltage in aqueous-based electrolytes that may enhance grid storage and zero-power transportation with high energy density in the future. At the same time, the realization of low-cost energy devices through the construction of cheap electrode materials deserves a permanent place in the market once the goals of high energy, extra power, and long cycling stability are achieved. Biomass-derived carbon retrieved from sources such as plants has attracted considerable attention because of the rich abundance, low cost, and environmentally friendliness. In addition, the utilization of porous hierarchical structures has achieved enhanced electrochemical performance with excellent capacitance, outstanding stability, and praiseworthy rate capability. However, issues still persist in procedures used to obtain biomass-derived carbon materials with a high yield and a high degree of carbonization/graphitization, surface functionality, and porous characteristics, wherein the materials are used as electrodes in ASC devices. The present review briefly addresses the need for biomass-derived carbon materials in ASCs, comprehensively categorizes SCs in the context of their historical background, and elucidates the SC mechanism. In addition, influencing factors, such as the pore size distribution, role of surface functional groups, surface area, active-material loading, heteroatom doping, and activation techniques used in the preparation of biomass-derived carbon, have been discussed in detail. Moreover, this review assesses other nanostructured carbon electrodes used in ASCs and advances made in the fabrication of ASCs by using biomass-derived carbon in aqueous electrolytes. Finally, existing challenges and mandatory solutions toward developing cost-effective and high-performance ASCs by using environmentally friendly biomass-derived carbon materials are discussed in detail.

1. Introduction

Energy is one of the most important factors that plays a vital role in society. The major forms of energy are being used at a faster pace, to meet the demand for electricity, than that required for overall energy consumption.[1] According to a recent report,[2] it was projected that the global electricity demand would reach around 38700 TWh by 2050; it was assessed to be 25000 TWh in 2017. In addition, India's electricity sector is dominated by fossil fuels, mainly derived from coal, which in 2017–2018 produced about three-quarters of all electricity in the country.[3] On the other hand, a National Geographic Society report clearly stated that 75% of people could face deadly heat waves by 2100 and there would be a rise in sea levels by 1 to 4 feet, unless carbon emissions were reduced. Electricity generation and transportation have become two major sources of CO_2 emission, leading to global warming.[4] As climate change concerns escalate and fossil fuel depletion becomes more imminent,[5] the world is moving toward the use of cost-effective and environmentally friendly renewable energy sources. It is expected that electric vehicles (EVs) with "zero emissions" will significantly contribute to solving the problems of global warming. As a result, the global EV market outlook for 2018 indicated that the global sales of EVs increased from 1.2 million in 2017 to 1.6 million in 2018, and is estimated to reach 2 million by the end of 2019.[6] The role of India in transforming itself to a net zero emission based energy system by 2050, as agreed at the Paris Climate Change Conference held in December 2015, will be keenly observed by the world in the coming years.[7] However, the main problem with renewable energy systems is that the profile of energy production and demand are mismatched.

To make the best use of intermittent renewable energy sources, we need to ensure the development of good electrical energy storage (EES) systems.[8] Over the past decade, electronic devices have transformed from being a novelty to indispensable in the modern world. The emergence of EVs has also improved the demand for EES devices.[9] Electrical energy can be stored in two fundamentally different ways: 1) indirectly through electrochemical energy storage in the form of batteries, and 2) directly through electrostatic energy storage in the form of capacitors and supercapacitors (SCs).[10,11] Unprecedented fast-growing technology and the increasing energy crisis have boosted the development of efficient EES systems, such as batteries and SCs. Batteries store energy chemically and hold s high energy density, however, they provide a low power density compared with SCs; thus leading to their preferred use in energy-storage applications. They also have a low cyclability and short life span due to the physiochemical changes that occur in electrodes and electrolytes during the charging–discharging process. Storing energy in batteries is not a viable solution because these devices lose their storage ability after 2–3 years,[12] as well as their associated environmental hazards and human safety issues. In addition, the power supplied by batteries is not able to cope with some power requirements, such as those needed in smartphones and automobiles. Growing interest in high power and energy density, safe, and eco-friendly energy-storage systems has placed SCs at the forefront of EES systems.

SCs or ultracapacitors are capacitors with large surface area electrodes separated by a small distance that can store 10 to 100 times more energy per unit mass/volume than that of

[a] M. L. Divya, Dr. S. Natarajan, Dr. V. Aravindan
Department of Chemistry
Indian Institute of Science Education and Research (IISER)
Tirupati 517507 (India)
E-mail: aravind.van@gmail.com
Homepage: https://aravindvan2.wixsite.com/aravindlab

[b] Prof. Y.-S. Lee
School of Chemical Engineering, Chonnam National University
Gwang-ju 61186 (Republic of Korea)
E-mail: leeys@chonnam.ac.kr

Supporting Information and the ORCID identification number(s) for the author(s) of this article can be found under: https://doi.org/10.1002/cssc.201901880.

electrolytic capacitors. They have a short charging time, high power capability, and long life cycle relative to batteries. SCs are capable of providing very high power density, which is nearly a thousand times larger than that of a battery. In addition, they can store energy 3 to 30 times lower than that stored by a battery.[13] SCs are fascinating devices that can be used for applications in which high power is needed and energy storage is less important. They can act as an excellent power source for applications in which batteries cannot be used, such as in cold weather, regenerative braking systems, and power bursts. Other applications of SCs, such as hybrid EVs and wind and solar energy harvesting, in addition to their use in trains and aircraft, are driving the global SC market at an advancing rate. Consequently, the compound annual growth rate has grown by 19.8%, in terms of revenue, and is expected to increase sixfold within the next decade.[14] The beauty of SCs is that charging can be performed within a few seconds and is durable for more than one million recharge cycles. SCs are also suitable for parallel combination with batteries, which provides high energy and power density to EESs. Technological innovations have steered the development of different types of SCs, including pseudocapacitors and capacitive, asymmetric, and hybrid capacitors with mixed features of batteries and SCs, because the global SC market is anticipated to witness a boom in the coming years.

Asymmetric supercapacitors (ASC) are SCs in which two dissimilar materials are assembled as the positive and negative electrode terminals; these can deliver a high power density relative to that of batteries and show comparable energy densities to that of lithium-ion batteries.[15] Among all materials available as an electrode in SCs, biomass-derived carbon (BDC) is the most suitable candidate due to its low cost, facile processing techniques, nontoxicity, rich abundance, environmentally friendly nature, high electronic conductivity, and impressive mechanical stability.[15,16] Most reviews published on SCs prepared with biomass-derived electrodes have focused on symmetric or single-electrode (three-electrode or half-cell) systems.[17–21] However, herein, we provide a comprehensive summary of recent research activities, mainly concentrating on capacitive ASCs prepared by using BDC as the active material.

Yun-Sung Lee is Professor at Chonnam National University, South Korea. He received his Ph.D. in 2001 from Saga University in Japan under the direction of Prof. Masaki Yoshio. He joined Chonnam National University in 2003 as Assistant Professor. He has authored and co-authored over 230 peer-reviewed publications and is an active member of the lithium battery and hybrid capacitor fields. He received the Yongbong Haksulsang, which recognizes a professor with excellent research achievement, in 2015. His research interests are in the fields of lithium batteries and sodium hybrid capacitors.

Vanchiappan Aravindan is currently working as Assistant Professor at the Department of Chemistry, IISER, Tirupati, India. He received his Ph.D. in 2009 from Gandhigram Rural University, Gandhigram, India. He then joined as Chonnam National University, Gwangju, South Korea, as a postdoctoral fellow with Prof. Yun-Sung Lee. Later, he joined (2010–2017) the Energy Research Institute at Nanyang Technological University (ERI@N), Singapore, as a senior scientist. His research interests include the development of high-performance electrodes and electrolytes for lithium-ion chemistry and beyond.

2. Supercapacitors

2.1. Historical background

SCs are growing at an exciting rate, mainly due to their use in smartphones, laptops, and tablet devices. An electrostatic capacitor or conventional capacitor is an energy-storing device that consists of two electrodes separated by a solid dielectric material. If the electrodes are connected to an external power source, positive and negative charges build up on the surface of the electrodes due to the difference in their potential. Charges remain on the electrode surface, even after removing the electric field, which is known as the charged state of the capacitor. During discharge, the positive and negative charges are released to the connected resistive load to deliver the stored energy.[22] Electrolytic capacitors are second-generation capacitors that use solid or liquid electrolytes with a separator between two symmetric electrodes. The third generation of capacitors is electric double-layer capacitors (EDLCs), which use carbon electrodes and store charge at the electrode–electrolyte interface.[23] The story behind the historical development of SCs starts with the demonstration of the first capacitor, a "Leyden jar", which consisted of a glass jar with two metal foils, water, and a conductive chain. Upon rotating this glass jar, static electricity can be produced. The concept of static electricity was understood at the start of the 19th century. In 1853, von Helmholtz introduced the first simple electric double-layer model. According to his model, charge separation takes place at the electrode–electrolyte interface. The electrode carries a charge density due to either an excess or deficiency of electrons at the electrode surface. The charge on the electrode surface is balanced by counterions present in the electrolyte. Therefore, the formation of two layers of opposite charges occurs at a separation distance of d (radius of the attracted ions). The behavior of the Helmholtz electric double layer is comparable to that of a parallel-plate capacitor and is capable of storing charge. However, this model fails to explain the dependence of the measured capacitance value on the potential or concentration of the electrolyte. Gouy, Chapman,

Stern, and Grahame explained the modern theory of EDLC in the late 19th and early 20th centuries.[24,25] Later, Gouy and Chapman first explained the thermal motion of ions near the charged surface of the electrode within the diffuse double layer.[24,25] This theory was only valid for low-concentration electrolytes. By combining these two models, Stern suggested a more realistic way of describing the physical situation at the electrode–electrolyte interface in 1924.[24,25]

The first electrochemical capacitor patent was applied for in 1957 by Howard Becker of General Electric.[26,27] However, this patent was not commercialized. An EDLC was made by using a porous carbon electrode and sulfuric acid as the electrolyte. In 1970, Standard Oil of Ohio (SOHIO) developed an electrolytic capacitor based on carbon electrodes.[25] Subsequently, Nippon electric company, NEC (Japan), licensed the patent from SOHIO and commercialized it in 1978.[28] In the early days of their discovery, SCs were used as backup memory for electronics. Advances in materials science led to the increased production of SCs with improved performance and lower rates. Numerous companies initiated the production of SCs in the late 20th century. The second type of electrochemical capacitor, termed as a pseudocapacitor with faradaic processes, was discovered in 1971.[25] One of the first designs of an ASC with a $Ni(OH)_2$-based positive electrode and an activated carbon (AC) negative electrode was proposed by MP Pulsar in 1989.[25] In 1992, Maxwell technologies manufactured their own SCs named Boost Caps.[22] To boost the production of high-quality, low-cost SCs to meet future demands requires enhanced research and development. However, extensive research is necessary to obtain a clear understanding of the basic mechanism for charge storage in EDLCs and pseudocapacitors.[25]

2.2. Electrical double-layer capacitors and pseudocapacitors

SCs are based on EDLCs, electrochemical pseudocapacitance, or a combination of both. SCs are power devices with an energy density of 5–10 Wh kg^{-1} and a high power density of about 10 kW kg^{-1}, which can be achieved for short durations.[29,30] The basic design of a SC consists of two electrodes, current collectors, a separator (ion-permeable membrane), and an electrolyte. The electrodes are made up of a metallic collector composed of a high surface area active material. Based on the storage mechanism and active material present in the electrode, SCs can be classified into two types, EDLCs and pseudocapacitors (or redox SCs; Figure 1). The capacitance of SCs is mainly due to surface reactions that occur on the electrode materials; these can be electrochemical adsorption or desorption of ions at the interface of electrodes and electrolyte in the case of EDLCs or faradaic surface redox reactions in pseudocapacitive materials.[31]

EDLCs, the most common type of SC, use high surface area carbon as the active material and double-layer capacitance as the charge-storage mechanism. In EDLCs, the electric double layer is formed between the electrodes, and the electrolyte acts as the dielectric medium. EDLCs can store charge electrostatically through the reversible adsorption of ions in the electrolyte onto the active material.[25,33,34] Ion adsorption and desorption is the mechanism for charging and discharging in EDLCs. No faradaic reaction occurs on the surface of the electrode, which means there is no charge transfer between the electrode and electrolyte at the interface.[25] The capacitance of an EDLC electrode can be calculated by using Equation (1):

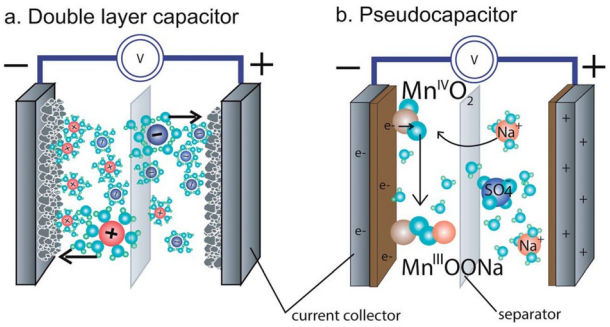

Figure 1. Schematic representations of a) an EDLC with carbon as the active material and b) a pseudocapacitor with MnO_2 as the active material (reproduced with permission from Ref. [32]; copyright Royal Society of Chemistry, 2014).

$$c = \frac{\varepsilon_r \varepsilon_0}{d} A \quad (1)$$

in which ε_r represents the dielectric constant of the electrolyte; ε_0 is the permittivity of vacuum; A is the ion-accessible surface area of the electrode material; and d is the Debye length, which is the distance between the ion center and the carbon surface. Compared with conventional dielectric capacitors, EDLCs can store more energy due to factors such as the high value of the effective surface area and very small charge-separation distance. The Helmholtz double-layer thickness at the electrode–electrolyte interface is in the range of 0.3–0.8 nm.[31] The time required for the formation of the double layer is in the order of 10^{-8} s, whereas the redox reactions for pseudocapacitors take between 10^{-2} to 10^{-4} s. Hence, EDLCs can respond quickly to potential changes, in comparison with faradaic capacitors.[25] The thickness of the electric double layer depends on the concentration of the electrolyte, size of ions, and solvation shell. The operative value of the double-layer thickness is 5–10 Å. In recent years, carbonaceous materials have been widely used as the electrode material for EDLCs because they can assure high power density, good cyclic stability, and can exhibit rectangular cyclic voltammograms and linear galvanostatic charge–discharge (GCD) profiles (Figure 2). AC, which has a large specific surface area (SSA) of 3000 $m^2 g^{-1}$, can yield a capacitance of about 145 F g^{-1}. Charge storage in rechargeable batteries and pseudocapacitors takes place through redox reactions between metal ions in the active material of the electrode. However, the difference is that the charging mechanism is controlled by cation diffusion within the crystalline framework of the active material in the case of rechargeable batteries. Capacitive and pseudocapacitive behavior are not under control of the diffusion mechanism. Faradaic reactions include oxidation–reduction, intercalation processes, or electrosorption between the electrode and electrolyte. Transition-metal oxides

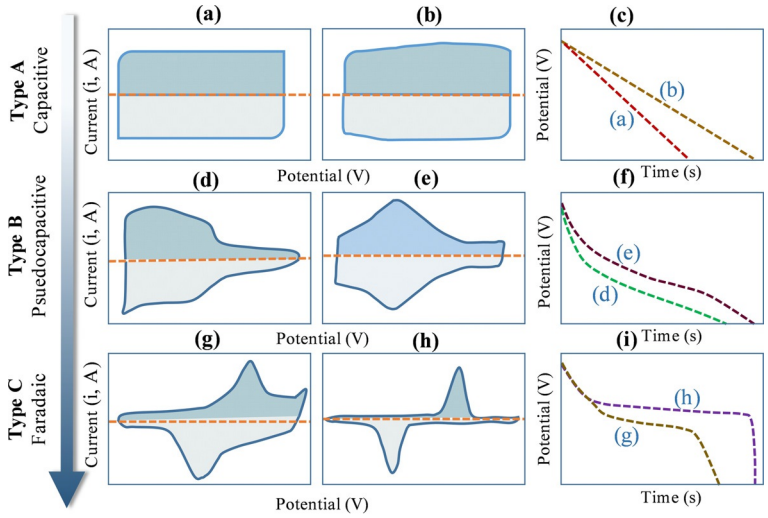

Figure 2. Typical CV traces (a, b, d, e, g, and h) and galvanostatic discharge curves (c, f, and i) obtained for various kinds of energy-storage materials. Type A: Capacitive types of a) EDLCs and b) surface redox materials (MnO_2 in aqueous electrolyte). Type B: Pseudocapacitive types of d) intercalation-type materials (lithium insertion into Nb_2O_5 in organic electrolytes) and e) intercalation-type materials with broad reversible redox peaks (Ti_3C_2 in acidic or aqueous electrolytes). Type C: faradaic types of battery-like materials (g–i).

and electronically conducting polymers are examples of the active materials used in pseudocapacitors and their capacitance value usually ranges from 300 to 400 $F\,g^{-1}$; however, they have a serious problem in regard to their long-term stability.[28,29,35]

EDLCs differ from pseudocapacitors and batteries, which both use faradaic reactions to store charge.[36–38] The term pseudocapacitance can be used to describe the behavior of electrode materials with the electrochemical signature of a capacitive electrode. Pseudocapacitance arises at the electrode surface and involves the passage of charge across the double layer, as in the case of batteries. However, the capacitance arises for thermodynamic reasons with respect to charge acceptance and a change in potential.[39,40] The charging mechanism is related to electron transfer due to the change in the valence state of the electrode material, rather than ion accumulation in the electrochemical double layer found in EDLCs. RuO_2 and MnO_2 are perfect examples of pseudocapacitive materials, which clearly show EDLC-like curves in CV and GCD measurements.[15,39] The capacitance in these materials originates from the linear dependence between the charge difference (ΔQ) and change in potential (ΔU). The charge-storage mechanism in pseudocapacitive materials is intermediate between that of pure electrostatic EDLCs and the diffusion process dominated by faradaic reactions in battery-type materials.[25] Pseudocapacitance is contributed to by active centers located at a distance of $<(2Dt)^{1/2}$, in which D is the coefficient of diffusion and t is the time of diffusion.[25,41]

The development of pseudocapacitive materials, the mechanisms involved in this behavior, and the materials that exhibit this behavior have been reviewed.[42] Incorporating a pseudocapacitive material into an EDLC electrode can result in a dramatic improvement in electrode performance. The different faradaic reaction mechanisms that give rise to electrochemical capacitive characteristics were identified by Conway et al.[43,44] and include underpotential deposition, redox pseudocapacitance, and intercalation pseudocapacitance (Figure 3).[40,45] Underpotential deposition occurs as a result of the deposition of metal ions onto the 2D metal–electrolyte interface at a potential above their redox potential. The voltage applied should be less than the redox potential of the cation. During this process, the operating voltage window is in the range of 0.3–0.6 V and the capacitance values are dependent on voltage. Hence, the energy density values are limited in underpotential systems, relative to other pseudocapacitive systems. Redox pseudocapacitance is based on the electrochemical adsorption of ions onto the surface or near the surface of the electrode material. These redox reactions use electron transfer between different oxidized species, such as RuO_2, MnO_2, or p-doped conductive polymers, and reduced species, such as $RuO_{2-x}(OH)_x$, $MnO_{2-x}(OH)_x$, or n-doped conductive polymers. By considering factors such as the reactant ions

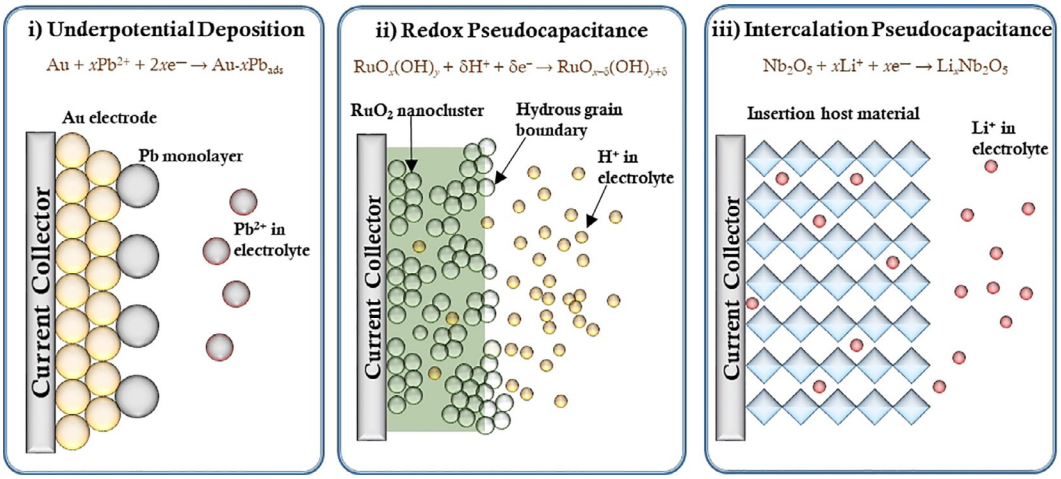

Figure 3. The different faradaic mechanisms that give rise to pseudocapacitance.

and density of the reactant sites, a redox pseudocapacitor can produce a maximum capacitance of about 5000 F cm^{-3}, whereas 1 cm^3 of a carbon-based EDLC can produce only a maximum capacitance of 825 F g^{-1}.[25] Intercalation pseudocapacitance occurs in the case of ion insertion/intercalation into layered redox-active materials, along with faradaic charge transfer without a change in the crystallographic phase. The electrochemical performance of an intercalation pseudocapacitor is midway between that of lithium-ion batteries and SCs.[46] Capacitor-type electrochemical signatures of such materials include fast ion transport, short charging time, high rate capability, and long cyclability.[25]

2.3. Symmetric, asymmetric, and hybrid SCs

As discussed earlier, pseudocapacitors show a higher capacitance due to additional charge transferred within a given potential window for two types of capacitors. However, they have a shorter life cycle and exhibit active-material degradation due to faradaic reactions.[15] As already mentioned, EDLCs offer high power density and good cycling stability. Asymmetric capacitors can be made by combining electrostatic EDLCs and electrochemical pseudocapacitance electrodes, which can produce 3 to 10 times higher capacitance than that of an EDLC.[28] Usually, SCs can be categorized into symmetric and asymmetric SCs based on the active material used in both electrodes. Symmetric supercapacitors (SSCs) use the same active material in both electrodes, either EDLCs or pseudocapacitive materials, which operate on the same fundamental principle of charge storage.[47] To increase the energy density of SSCs with an aqueous electrolyte, ASCs were developed. The term hybrid supercapacitor (HSC) is a type of ASC, which means the pairing of two electrodes with different charge-storage mechanisms, mainly one capacitive-type electrode and the other a battery-type electrode, and the performance of the HSC is at midway between the battery and SC performances. SSCs can be classified into two types, symmetric HSCs and capacitive symmetric SCs. SSCs with hybrid behavior represent two identical carbonaceous electrodes, with an electrochemically active molecule used as the electrolyte, such that faradaic reactions occur on the surface of one of the electrodes, giving a battery-type charge-storage mechanism. Scheme 1 provides an overview of different types of SCs.[25,36,47]

3. Asymmetric Supercapacitors

An ASC is based on two different electrode materials, of which one is based on redox reactions (faradaic/faradaic-like) with or without non-faradaic reactions and the other electrode is based on electric double-layer (non-faradaic/electrostatic) adsorption/desorption. The wide application of SSCs is mainly held back by their low energy density and narrow operating voltage window. The working voltage in an SSC with an aqueous electrolyte is limited to <1 V due to water splitting or the thermodynamic breakdown of water molecules. The thermodynamically stable voltage window of a water molecule is 1.23 V. However, few reports are available to enhance the energy density of the SCs by optimizing the surface charge and enlarging the potential window higher than 1 V; thus demonstrating that there is always unused potential beyond the upper and lower limits of potential based on aqueous SSCs.[48,49] In addition, some promising strategies, such as exploiting the "water-in-salt" electrolyte, adjusting the pH of the electrolyte, modifying the surface of the electrode, and introducing redox-active additives, are considered to be effective tactics for maximizing the operating voltage of the SCs. However, the fabrication of

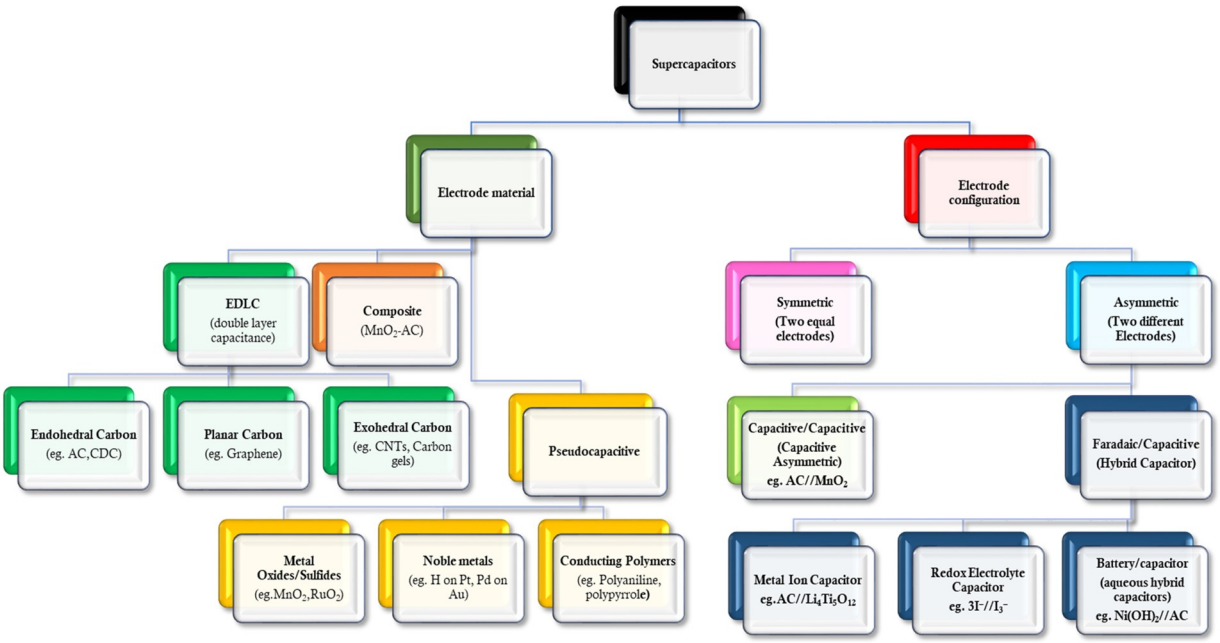

Scheme 1. Classification of SCs based on the charge-storage mechanism and type of active materials used in both electrodes. CDC = carbide-derived carbon, CNT = carbon nanotube.

ASCs is more convenient and they are possible to operate beyond 2 V with conventional aqueous electrolyte, as clearly highlighted by Yu et al. in their recent review.[50] In SSCs, both electrodes are made from the same active material with equal mass loading. Hence, the operating potential window of a SC only covers the narrow potential range of the single active material. The potential window of SSCs can be increased by using organic electrolytes. Organic electrolytes have good electrochemical stability and offer a wide potential window of 2.5–4 V, but they have a high equivalent series resistance (ESR), low ionic mobility, and low diffusion rates, which lead to a reduction in both the capacitance and power density. The decomposition of organic electrolytes also leads to pollution and other safety issues. Aqueous electrolytes are low cost, eco-friendly, and can provide high capacitance and power density. The operating voltage window of aqueous electrolytes depends on the capacitive potential range of the electrodes used.[50] The type of electrode material and electrolyte play a vital role in determining the potential window of an aqueous electrolyte based SC. This has led to the development of asymmetric systems, which can give a voltage of 2 V with aqueous electrolytes. ASCs cover a large group of SCs because they can be constructed from two electrodes of the same nature, but different mass loadings, or two electrodes of different materials.[51] ASCs can also be formed from two different carbonaceous materials as the positive and negative electrodes (e.g., AC and graphene) or the same material with different mass loadings, such that the electrostatic charge-storage mechanism will occur at both electrodes. ASCs can also be formed with one carbon material and another pseudocapacitive material. These two types of ASCs will fall into the group of capacitive ASCs. Hybrid ASCs were developed by combining a capacitive electrode with a battery electrode.[26] The charge-storage mechanism in both electrodes of the ASC may or may not be the same.[15,25,47] The concept of ASCs is considered to be one way to solve the issues of SSCs, especially the energy density. ASCs can achieve a wide operating window because they combine the advantages of both positive and negative electrode materials.[25] As a result, the ASC configuration is considered to be a promising approach to improve the energy density of electrochemical capacitors.

3.1. Performance of ASCs

SC performance can be analyzed by using certain parameters, such as the specific capacitance (*C*), operating voltage (*V*), ESR, cycling stability, time constant, energy density, and power density. Cyclic voltammetry (CV), GCD, and electrochemical impedance spectroscopy are conventional electrochemical techniques used to characterize SC performances. The amount of charge stored in an electrode under a given voltage is given by the capacitance ($\Delta Q/\Delta U$). Specific capacitance, another important parameter, refers to the capacitance per unit mass/volume of active material. GCD or CV are commonly used to determine the specific capacitance.

The capacitance (*C*) observed from the GCD curve can be calculated by using Equation (2):

$$c = \frac{I}{\mathrm{d}V/\mathrm{d}t} \tag{2}$$

in which *I* is the discharge current and $\frac{dV}{dt}$ is the slope of the GCD curve. In the case of faradaic electrodes, the GCD curves are not linear and the capacitance can be calculated from CV data by using Equation (3):

$$c = \frac{\int I\mathrm{d}V}{v\Delta V} \tag{3}$$

in which *I* is the discharge current, *v* is the scan rate, and ΔV is the potential range. The specific capacitance of a single electrode can be calculated from the capacitance value by using Equation (4).

$$C_s = \frac{C}{\pi} \tag{4}$$

in which π is the effective weight, area, or volume. If C_s represents a single electrode, π corresponds to the active material of the electrode. If C_s represents the total device, the active materials present in the entire system need to be considered.

The energy density of a SC is the quantity of energy stored in the SC per unit mass. For EDLCs and pseudocapacitors, this can be calculated by integrating the GCD curves [Eq. (5)].

$$E = \int Q\mathrm{d}v = \int_0^{V0} CV\mathrm{d}v = \frac{CV^2}{2} \tag{5}$$

For a battery-type electrode, in which the GCD is not linear, the energy density can be calculated from the CV curve by using Equation (6).

$$E = \int_{t_1}^{t_2} IV_{(t)}\mathrm{d}t \tag{6}$$

in which t_1 is the time after the initial *IR* drop, t_2 is time at which the discharge is finished, and *I* is the applied current. The power density of the SC is governed by the energy that is delivered per unit time. In comparison with electrolytic capacitors and batteries, SCs can provide a high power density. The maximum power of a SC can be determined from the maximum potential value and ESR by using Equation (7).

$$P_{max} = \frac{V^2}{4\mathrm{ESR}} \tag{7}$$

ESR is one of the key parameters that determine the power density and overall performance of an electrode. ESR depends on 1) the intrinsic electronic resistance of the active material and current collector, 2) the contact resistance between the active material and the current collector, 3) the electrolyte ionic resistance, and 4) the ion transport resistance across the separator.

The total quantity of charge stored on the surface of each electrode is given by Equation (8), which is the product of the specific capacitance, mass of active material, and potential window of each electrode used to obtain a charge balance, $Q^+ = Q^-$.

$$Q_{electrode} = C_{electrode} m \Delta E \quad (8)$$

To obtain the optimal performance of an ASC, the mass ratio of the electrodes can be adjusted [Eq. (9)].[25,27]

$$\frac{m_+}{m_-} = \frac{C_{electrode-} \times \Delta E_-}{C_{electrode+} \times \Delta E_+} \quad (9)$$

A Ragone plot can be used to compare the performance of different energy-storing devices. The specific energy values ($Wh\,kg^{-1}$) are plotted against specific power ($W\,kg^{-1}$). Both axes will be preferably displayed on a logarithmic scale, which helps to plot very low and high values on the same graph. Figure 4 shows the anticipated electrochemical performance of an ASC, which shows high energy and power density.

A summary of factors used to compare the operation of SSCs and ASCs in different configurations is given in Table 1.

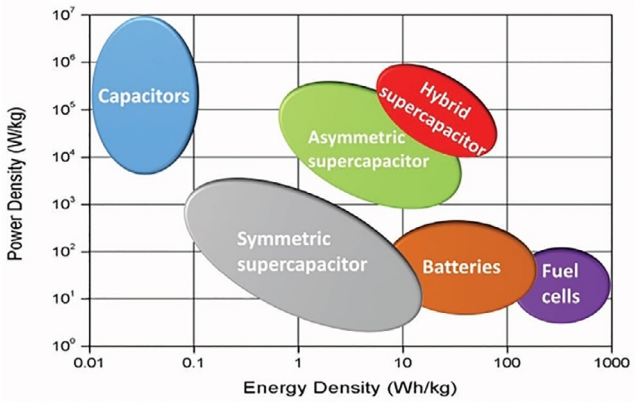

Figure 4. A Ragone plot used to compare the energy and power density values of various SCs and batteries with ASCs (reproduced from Ref. [15]; copyright Wiley-VCH, 2017).

4. Materials Used in SC Electrodes

SCs have a wide range of applications as energy-storage systems and power sources in EVs; smart grids; consumer electronics; and, most importantly, uninterruptible power supplies.[52,53] In general, SCs have energy densities lower than that of batteries. Currently, tremendous research efforts have been focused on methods and materials that can increase the energy density of SCs. SCs contain two positive and negative electrodes, a separator, and an electrolyte. By increasing the specific capacitance and operating voltage window, or decreasing the value of ESR, the energy density and power density of SCs can be improved.[54] ASCs are considered to be a win–win system in which the benefits of batteries and SCs are brought together in one system. In this EDLC, the capacitor-type electrode serves as a power source and the battery-like faradaic electrode serves as an energy source. To realize a high energy density in ASCs, the operating potential window should be wider. The selection of two electrode materials with the largest difference in work function can provide a wider operating voltage window in ASCs.[15]

From a materials point of view, different materials can be used as the electrodes in ASCs. The factors that decide the suitability of an electrode material are 1) high SSA; 2) ionic conductivity; 3) chemical, thermal, and mechanical stability; 4) excellent corrosion resistance; 5) optimum pore size distribution (PSD); 6) low-cost and availability; and 7) nontoxicity. In the case of EDLCs/pseudocapacitors, charge storage takes place at or near the surface of the electrode material. The use of an electrode material in its nanoform can result in a higher surface to volume ratio, which eventually increases the surface area. Decreasing the particle size can enhance the complete utilization of active material, that is, 100% participation in electrochemical performance.[29] Low ionic or electronic conductivity can lead to a high ESR value, which, in turn, lowers the specific capacitance. Electronic conductivity can be enhanced by using binder-free electrodes (e.g., carbon cloth, CNTs) and highly conductive metal composites. The direct fabrication of the active material on the current collector is one of the viable approaches used to improve the cycle life.[15,52] Cycling stability depends on the mechanical and chemical stability of the elec-

Table 1. The specific capacitance, energy density, and power density of SSCs and ASCs.

Configuration	Equations	Definition of symbols
three/single electrode	specific capacitance $C = \frac{I\Delta t}{m_1 \Delta V}$	m_1 = mass of active material in the working electrode m_2 = mass of active material in any one electrode m_3 = total mass of active electrode material in the positive and negative electrode I = discharge current Δt = time of discharge ΔV = potential drop during the discharge/potential window C = specific capacitance E = specific energy P = specific power
two-electrode symmetric	specific capacitance: $C = 2\left(\frac{I\Delta t}{m_2 \Delta V}\right)$	
	energy density: $E = \left[\frac{C(\Delta V)^2}{8}\right]$	
	power density: $P = \frac{E}{\Delta t}$	
two-electrode asymmetric	specific capacitance: $C = \left(\frac{I\Delta t}{m_3 \Delta V}\right)$	
	energy density: $E = \left[\frac{C(\Delta V)^2}{2}\right]$	

trode material and, of course, on the thermodynamic stability of the electrolyte.

Hybrid electrochemical storage systems are becoming an attractive alternative to conventional EDLCs or pseudocapacitors by incorporating a battery-like electrode (source of energy) with a capacitor-like electrode (source of power) inside the same cell. The use of a suitable combination of electrode materials can widen the operating voltage window of an ASC, which can lead to further improvements in the energy and power density of the system. Different combinations of positive and negative electrodes have been studied in the presence of different electrolytes to analyze their performance. An electrode with a faradaic-type charge-storage mechanism can increase the energy density, but will negatively influence the cyclability of the electrode. There should be an appropriate balance between the different performance characteristics of ASCs, which strongly depend on the combination of electrode materials used.[29]

Negative electrode materials commonly used in ASCs include carbon-based materials (AC, CNTs, and graphene),[15] metal oxides (Fe_2O_3, MoO_3, WO_3, MnO_2,[55] In_2O_3,[56] and Bi_2O_3),[57] and metal nitrides (TiN, VN, Mo_2N, and WON). The positive electrode material used in ASCs should exhibit pseudocapacitance as a result of a faradaic charge-transfer mechanism or electrosorption/desorption of the electrolyte ions with the electrode. Compared with the EDLC mechanism, pseudocapacitance can offer high specific capacitance and energy density values. The positive electrode materials most widely used in ASCs include conductive polymers (polyaniline, poly(3,4-ethylene dioxythiophene), polythiophene, and polypyrrole) and metal oxides (RuO_2, MnO_2, V_2O_5, and $Ni(OH)_2$).[15] Among these, MnO_2 is the most commonly used positive electrode material in ASCs because of its combination of negative EDLC carbon material electrodes and an aqueous electrolyte, which can reach a potential window of 2 V due to the combined effect of high surface area carbon and water decomposition overvoltage on MnO_2.[58] EDLC electrodes with biomass-based carbon and a MnO_2 positive electrode are becoming a suitable combination for use as low-cost electrodes in ASCs. The use of nanostructured MnO_2 can lead to further improvements in the electrochemical performance of ASC-based systems.[29] Carbon-based materials can also be used as a positive electrode material in ASCs, as shown by Ma et al.[59] Apart from this, other crucial factors, such as the active material loading, surface area, and activation technique, are pivotal to attaining high electrochemical performance, as clearly described in the following sections.

4.1. Active material loading

A Ragone plot can provide the performance level of batteries and SCs, in terms of their energy and power densities. These two parameters are essential for any energy-storage device. In the case of an electric car, the energy density shows the distance it can travel after a single charging process and the power density shows the speed with which the car can travel. Generally, SCs provide a high power density, long cyclability, and low energy density compared with that of batteries, but a commercial SC can deliver more energy over a smaller time frame. Usually, ASCs can exhibit higher energy densities than those of symmetric configurations, but the increase in the energy density of a SC can only be achieved at the expense of the power density or cyclability of the device. The energy and power density of a SC can be represented on both gravimetric and volumetric bases (Figure 5). Presenting these values by considering only the mass or volume of the active material may not provide the correct performance of the device.[60] However, to obtain a clear picture of device performance, it is very important to consider the other components in the device, such as current collectors, electrolyte, separator, and binders. The contribution of carbon materials in a packaged commercial SC is only 30% of its total mass. Therefore, the energy and power density of an assembled SC device will be equal to nearly one-third to one-quarter of the energy and power density of the active materials present in the device. This correlation also has an effect on the thickness and density of the active materials present in the system. In addition, the benefits of carbon materials cannot be translated to large-scale devices if thin-film or low-density electrodes are used.[61] Whenever the thickness of the nanoporous carbon material increases, there is an additional drop in the capacitance value by half or one-third of its actual value.[62] Hence, the thickness or mass of the active material in a SC device plays a major role in deciding the overall performance of the device.

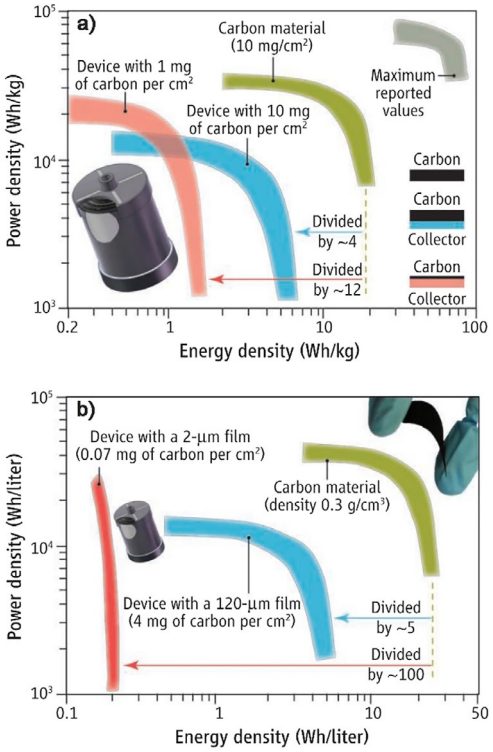

Figure 5. The influence of active material loading on the a) gravimetric and b) volumetric performance analyses of energy-storage systems (reproduced with permission from Ref. [61]; copyright American Association for the Advancement of Science, 2011)

The two-way representation of power and energy density in a SC device creates uncertainty in the performance level of SCs. The use of low-density carbon materials, such as nanotubes or graphene, can lead to the formation of empty space within the electrode, which will be filled up with electrolyte and result in an increase in the weight of the device without increasing the capacitance. Gravimetric energy density values are irrelevant in the case of SCs prepared with thin carbon film because the weight of carbon active material is negligibly small. However, it may exhibit a high gravimetric power density and discharge rate values, which cannot be scaled up linearly with the thickness of carbon material used. To solve existing problems in energy-storage systems, we need to develop new low-cost, high-performance electrode materials, and it is essential to establish a standard method for the presentation of energy and power density of SC devices.

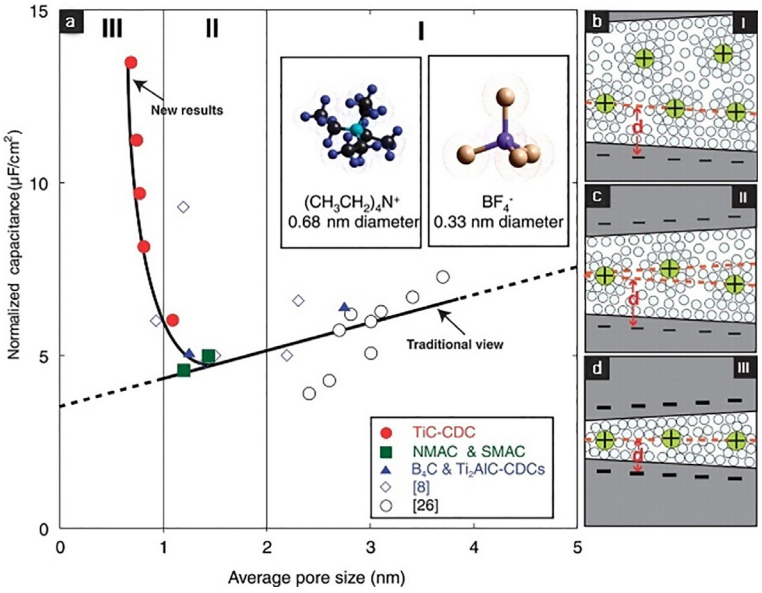

Figure 6. Normalized capacitance versus average pore size for carbon materials reported in the literature and tested in the same electrolyte. a) Plot of specific capacitance normalized by BET SSA for the carbons in this study and in two other studies with identical electrolytes. The normalized capacitance decreased with decreasing pore size until a critical value was reached, unlike the traditional view, which assumes that capacitance continually decreases. It would be expected that as the pore size becomes large enough to accommodate diffuse charge layers, the capacitance would approach a constant value. b–d) Drawings of solvated ions residing in pores with distance between adjacent pore walls b) greater than 2 nm, c) between 1 and 2 nm, and d) less than 1 nm illustrate this behavior schematically (reproduced with permission from Ref. [64]; copyright American Association for the Advancement of Science, 2006).

4.2. Pore size distribution

Carbon materials with bimodal porosity (a combination of micro- and either meso- or macropores) are believed to be suitable materials because energy storage mainly takes place in the micropores, which constitute the majority of the surface area, whereas large pores are actively involved in mass transport. Hence, it is important to have some control over the porosity, which can alter the charge-storage capability of carbonaceous materials.[34] Porous carbon produced by using traditional methods from natural or synthetic precursors does not provide a favorable distribution of pore structures.[63] To achieve the maximum capacitance from carbon materials, the pore size should be greater than the size of the electrolyte ion and solvation shell. CDC materials are a class of porous carbon materials, produced through high-temperature chlorination of carbides, which possess 50–80% open pore volume.[63] Furthermore, it can be considered as a suitable candidate for studying the effect of the PSD in carbon materials used for SC applications, for example, it possesses a narrow PSD with tunability and an SSA of about 2000 $m^2 g^{-1}$. In addition, it may also produce good capacitance if used as an active material in SC electrodes with different electrolyte systems. Chmiola et al. used titanium carbide-derived carbon (TiC-CDC) as the active material in a SC electrode in contact with H_2SO_4 electrolyte, and reported the relationship between micropore size and capacitance.[64] An unusual increase in the capacitance value of carbon material was observed at a pore size of <1 nm (Figure 6). For TiC-CDC, increasing the pore size had an unfavorable effect on the normalized capacitance. There was also a tendency to low capacitance for pore sizes of <1 nm. These studies reported that this size effect was independent of the carbon material used, but this statement was not true for pore sizes less than the critical value, such that the normalized capacitance increased with a decrease in the pore size. Region I in Figure 6a represents the variation in the normalized capacitance with pore size if the pores are twice the size of that of the solvated ions (Figure 6b). The researchers explained that compact layers of ions present near the wall of the pores contributed to the capacitance in this case. If the pore size is less than twice that of the size of the solvated ions (Figure 6c), there is a decrease in the value of the normalized capacitance, as shown in region II in Figure 6a. This was attributed to a reduction in the area available for double-layer formation, which, in turn, could reduce the specific capacitance. This may also be the reason for the reduction in the specific capacitance observed with the decrease in the pore size larger than 1 nm. However, upon further decreasing the pore size, such that the size of the pore is less than that of the size of a solvated ion (Figure 6d), there is a rapid increase in capacitance, as shown in region III in Figure 6a. It was concluded that there was an increase in the normalized capacitance if the crystallographic diameter of the ions matched that of the pore size. Hence, it is necessary to design carbon materials with a high volume of narrow, short tunable pores to produce SC electrodes with high energy and power density.

4.3. Surface functional groups

The surface chemistry of carbon materials is an important factor that decides the usability of carbon in SC applications. Surface functionalization is one of the effective methods used

to enhance the capacitive performance of carbon materials. The distribution of surface functional groups in carbon materials depends on the composition of the precursor and conditions used in their synthesis.[65] Franckowiak et al. explained that the presence of surface functional groups could modify the electronic properties (electron-donor or -acceptor properties) of carbon materials, which, in turn, could affect the EDLC charging mechanism and induce pseudocapacitance faradaic reactions.[66,67] Based on the precursor and/or conditions used in their preparation, carbon materials can contain a variable number of foreign elements or heteroatoms, such as oxygen, nitrogen, sulfur, and hydrogen. The functional group distribution on the surface depends on the pore size of the carbon material and precursor.[68] Studies have shown that nitrogen- and oxygen-containing functional groups can enhance the metal-ion uptake capability of carbon materials.[69] Of these, nitrogen-containing carbon materials have been widely explored as electrode materials in SCs.

The role of nitrogen groups in graphene on the capacitance behavior of AC was studied by Lota et al.[70] Nitrogen atoms present in carbon can be categorized into three types: pyridinic, pyrrolic, and quaternary nitrogen atoms. Of these, pyridinic (N6) and pyrrolic (N5) are considered more suitable for SC applications in which nitrogen atoms positioned at the edges of the graphene layers can produce a pseudocapacitance effect.[71,72] Quaternary nitrogen atoms carry a positive charge and can enhance the transfer of electrons in carbon materials.[31,73,74] Oxygen-containing functional groups on AC (mainly COOH and C=O) can be derived by the activation of porous carbon or electrochemical oxidation techniques. Some of these groups are electrochemically active and involved in the enhancement of EDLC capacitance (pseudocapacitance due to the faradaic reactions of these groups). Based on the nature of the C–O bond, these oxygen-containing functional groups can be categorized into three types: 1) chemically fixed, such as carbonyl groups; 2) surface groups, such as carboxylic groups; and 3) surface groups with electrochemical redox activity, for example, quinine/hydroquinone moieties. Carbonyl groups are generally electrochemically inactive and cause a shift in the zero-point charges, whereas carboxylic groups impart acidity to the surface. It is found that only quinine-type surface oxygen groups are electrochemically active under acidic electrolytic conditions.[31] These redox-active functional groups can enhance both the capacitance and rate performance in aqueous electrolyte solutions. Oxygen-based functional groups are normally unstable and undesirable for carbon materials because most of them are degassed at temperatures $<800\,^{\circ}C$. They also have some negative effects on the reliability of capacitors, such as provoking self-discharge and causing current leakage and device degradation.[75] Oda et al. reported a comparison of the effects of specific functional groups in EDLCs with aqueous and organic electrolytes.[76] In the case of SCs, functional groups have an impact on the conductivity, wettability, ion diffusion, pseudocapacitance behavior, and stability of the active materials. Broad knowledge of selective functionalization is very important, so that unstable groups can be removed from the carbon surface and stable ones preserved to acquire maximum benefit from the surface functional groups in carbon electrode materials.[77]

4.4. Heteroatom doping

The surface electroactive sites in BDC play a vital role in determining the performance of an electrode.[78] The incorporation of these active sites can be carried out by using different methods, such as heteroatom doping, chemical activation of the biomass precursor, the incorporation of transition metals, or by using redox-active electrolytes. Doping heteroatoms into the carbon skeleton can effectively promote volumetric capacitance. However, it is important to optimize the degree of doping because excessive doping can lead to low conductivity. Some renewable biomass precursors are selected due to the natural abundance of heteroatoms such as N, O, B, P, or S.[79] The presence of heteroatoms such as O and N, and other functional groups on the carbon surface, can affect the pseudocapacitance behavior of an electrode.[80,81] Activation of a biomass precursor with KOH and NaOH can also generate oxygen active sites on the surface of the carbon material. In some cases, heteroatoms such as O and N are inherently present in the biomass precursors. By using different activating agents, sufficient heteroatoms can be induced on the surface of carbon materials. The adsorption and transportation of electrolyte ions can be improved by sulfur doping.[81] However, the presence of different heteroatoms can enhance electrode wettability, which can cause an increase in capacitance. Heteroatoms can also donate a pair of electrons, which causes a change in the charge and spin densities of the carbon atoms near the doped heteroatoms. As a result, a pseudocapacitive reaction is induced.[82,83] Generally, heteroatom-doped biomass-based carbon materials can be obtained by mixing the biomass precursor with other precursors containing heteroatoms or post-treatment of biomass with a suitable source of heteroatoms.[52]

4.5. Activation and activating agents

Common methods used to convert biomass precursors into AC include pyrolysis or hydrothermal carbonization (HTC) followed by activation by means of physical and chemical methods, or a combination of both.[33] In physical activation, the pyrolyzed precursor is exposed to high temperature ($>450\,^{\circ}C$), usually in the range of 600–1200 °C, under an atmosphere of steam, CO_2, or a mixture of both.[84] In chemical activation, the carbon precursor is subjected to a high temperature, ranging from 450 to 900 °C, and is impregnated with chemical agents, such as KOH, NaOH, H_3PO_4, H_2SO_4, ZnCl, and K_2CO_3.[52,75] By strict selection of the precursor or by using a suitable activation method, AC with homogeneous and controlled microporosity can be produced.[85]

Physical activation is a simple and green method used for the synthesis of AC, which is generally conducted at a higher temperature than that of chemical activation. CO_2 is the most commonly used physical activating agent. In addition to steam and CO_2, air can also act as a physical activating agent, but air

activation is usually performed at a lower temperature (< 500 °C). Air activation can have a notable impact on the porous properties of BDC.[52] However, AC produced through CO_2 activation is likely to have a high mesoporous fraction with an increased average pore size. This may be attributed to the large size of the CO_2 molecules, which prevents their accessibility into the micropores present in carbon materials. Researchers have also reported that CO_2 activation can cause a moderate degree of graphitization, with graphene sheets stacked in parallel in the structure of porous AC.[52,86] Steam is a low-cost, readily available activating agent that does not require a postactivation process for byproduct removal. However, AC formed by steam activation is normally less conductive due to the generation of oxygen-containing surface groups during the activation process. CO_2 and steam are more commonly used than air because they are capable of producing AC with a wider PSD. Researchers have also reported that steam activation produces AC with a larger fraction of meso- and macropores than that of CO_2 activation.[52]

Currently, chemical activation is preferred over physical activation due to its low activation temperature, shorter activation time, higher SSA, and more uniform PSD.[52,87] On the other hand, the main drawback of this method is the need for postactivation with acid washing to remove chemical impurities generated during the activation process. Different chemical activating agents can produce AC with various properties. KOH is most commonly used for the activation of BDC, which can produce carbon with a rough surface that, in turn, increases the SSA and porosity. Due to complex factors such as the permeation of the activating agent into the carbon skeleton and the reactivity of the carbon precursor, the mechanism of KOH activation is not fully understood. Generally, the mechanism of KOH activation of carbon materials is based on experimental observations and can be classified into three main mechanisms:[88] 1) chemical activation, that is, a redox reaction between carbon and KOH to create microporosity within the carbon skeleton; 2) physical activation, in which gasified products from the redox reaction, such as CO_2 and H_2O, further enhance the formation of porous structures; and 3) intercalation of metallic K into the carbon skeleton, which results in expansion of the carbon lattice. Different variables that affect KOH activation of a given carbon precursor and their normal range include the mass ratio of KOH/biomass (2 to 5), the heating rate (3–10 °C min^{-1}), temperature (550–900 °C), and time of activation (1–4 h). Based on the value of these parameters and type of carbon source, KOH activation can result in AC with increased SSA, uniform PSD, and controllable surface functional groups. In comparison with a single step, the two-step KOH activation method is often used to prepare BDC for SCs.[52,89]

Another commonly used chemical activating agent for BDC is $ZnCl_2$, which has deoxygenation properties at high temperature and can remove oxygen in the form of water or through carbothermal reduction. Therefore, it can act as a dehydrating agent during the activation process. AC obtained from $ZnCl_2$ activation generally shows a difference in the SSA value and the ratio between micro- and mesopores, compared with KOH and AC.[90] This activation method also requires postactivation washing with acid to remove the remaining Zn atoms.[34] Activation with H_3PO_4 usually results in a low SSA (< 1000 $m^3 g^{-1}$) relative to those with KOH and $ZnCl_2$. It is mainly used for biomass such as fruit stones, but acid phosphate groups may remain on the surface of the carbon material, which makes the activation process a balance between conductivity and surface functionality.[34] KOH activation is used for BDC-based SC electrodes because it can deliver a suitable PSD with a high value of SSA.[52]

4.6. Specific surface area

In the case of AC, only a fraction of the SSA can help to attain high energy storage. This is because of its poor pore size uniformity. The presence of micropores that are inaccessible to electrolyte ions and macropores result in a low surface to volume ratio. The combination of these two factors can result in a low specific capacitance. CNTs exhibit moderate surface area and high conductivity, but SCs based on CNTs do not exhibit optimum capacitance without the addition of pseudocapacitive material.[91] The amount of energy or charge stored is directly proportional to the capacitance of the material. An increase in capacitance is possible by increasing the carbon surface area, which can be achieved by choosing different carbon precursors or developing various synthetic procedures. However, there is no linear relationship between the surface area and capacitance of a carbon material.[92] An increase in the surface area of carbon materials is possible by introducing porosity into the bulk carbon material, which can form carbon particles within an internal porous network. Simon and Gogotsi explained the role of pore size and PSD in controlling the capacitance of carbon materials.[93] The surface charge-storage mechanism in EDLCs allows the rapid charging and discharging of a SC device. The faradaic efficiency, which is the ratio of time taken for discharging and charging the SC at the same current, is nearly 100% for SCs, which also ensures the high cyclability of the device.[93]

4.7. Self-discharge

SCs are generally used only for short-term energy storage due to their self-discharge process, which is a spontaneous drop in voltage between two EDLC electrodes if left under an open-circuit condition for long-term storage.[94] This was first explained by Conway et al.,[95,96] who proposed three main mechanisms for the root cause of self-discharge. 1) Overcharging: if the electrode potential is greater than the stable potential window of the electrolyte solution, electrolyte decomposition (faradaic reaction) takes place at the electrode–electrolyte interface until the voltage reaches the stable potential window of the electrolyte. Gases produced during this process may block the pores present on the surface of the electrodes and separator, which, in turn, causes fading of the capacitance due to a drop in the SSA of the electrodes. Overcharging can also lead to a rise in the ESR value and reduce power capability. 2) Side reactions: redox impurities present in the electrolyte or on the surface of the electrode material may result in parasitic faradaic reactions,

which eat away at some of the charge stored in an EDLC. The presence of traces of H_2O in organic electrolytes can narrow its electrochemical window. Studies have reported that the surface functional groups present on the surface of carbon electrodes may also contribute to capacitance fading, even though they are responsible for pseudocapacitance. Furthermore, it is believed that the degree of leakage current may depend on the type of electrolyte used and the presence of active functional groups on the electrode surface.[53] However, neutral aqueous electrolytes generally cause minor leakage. 3) Ohmic leakage: leaky bipolar electrodes can lead to internal ohmic leakage pathways between the positive and negative electrodes. The model reported by Conway et al. indicates that self-discharge due to different mechanisms will accomplish diverse potential fading rates and all of these processes can lead to a reduced open-circuit potential and loss of stored energy in charged EDLCs.[96,98]

5. Carbon-Based Materials Used as Electrode Materials for ASCs

Humankind has witnessed the stone age, bronze age, and iron age. The 20th century is known as the silicon age. Based on events in the first decade of the 21st century, it may be known as the carbon age. Carbon is the most versatile element in the periodic table and has become the building block for almost all of the main energy-storage devices reported to date. Carbon materials play a vital role in the development of cheaper and cleaner energy-storage methods.[15,99] Taking a suitable starting material and selecting appropriate processing routes can allow several modifications to be performed on carbon-based materials.[100] More than 95% of commercialized SCs use carbon as the active material.[93]

Carbon materials can be categorized into soft carbon and hard carbon. Soft carbon (or graphitizable carbon), such as pitch-based chemicals (coal tar, petrol pitch, and organic polymers), can be easily graphitized at temperatures $<2000\,^{\circ}C$, whereas hard carbon is non-graphitizable carbon, such as phenolic resin, carbohydrates, and biomass, which are difficult to graphitize, even at $3000\,^{\circ}C$.[34] Carbon materials are widely used because of their availability in different forms (including fibers, powders, nanotubes, and nanospheres) and their wide range of dimensionality.[54]

In aqueous ASCs, high energy and power density can only be achieved through the development of appropriate electrode materials. Carbon-based materials (or carbonaceous materials) can be used as the active material in both negative and positive electrodes in ASCs. However, their action mechanism is different in both cases. The most commonly used carbonaceous materials include porous carbon (AC and nanoporous carbon), CNTs (single-walled CNTs and multiwalled CNTs (MWCNTs)), and graphene (or reduced graphene oxide (rGO)). Carbon-based materials are the most suitable candidates for use in the negative electrode in ASCs and can act as EDLCs. Optimum performance can be achieved due to properties such as large SSA, high electrical conductivity, controllable porosity, and surface chemistry of carbon. The action of carbon-based materials used as a negative electrode material can be explained by Equation (10):

$$\text{Carbon} + M^{+} + e^{-} \leftrightarrow \frac{\text{Carbon}}{M} \qquad (10)$$

in which M^{+} is a metal cation. Moreover, carbonaceous materials have high rate capabilities, enhanced cycle stability, and can be operated at high charge and discharge rates with a lifetime of over a million cycles. Hence, the main focus of current research is on the development of suitable electrode materials for SCs without sacrificing electrochemical performance.[52] In the recent past, the mechanism of energy storage in carbon electrodes has been studied and the relationship between the properties of carbon materials and specific capacitance has been proposed.[101] To increase the amount of charge stored in carbon materials, it is necessary to increase the surface area, which is possible by choosing different carbon precursors or adopting various synthetic protocols. The surface area can be increased by increasing the porosity of the carbon material. However, as mentioned above, there is no linear relationship between surface area and specific capacitance of carbon materials. Importantly, PSD and tuning the porosity of carbon materials have a significant role in the capacitance.[101]

Different carbonaceous materials have been used as the negative electrode in ASCs, including porous carbon, CNTs, and graphene. Among them, AC stands out because of its large surface area ($>1000\,m^2\,g^{-1}$), large pore volume ($>0.5\,cm^2\,g^{-1}$), and relatively low cost. Consequently, AC is the most widely used active material in EDLCs. AC also has a broad pore size tunability, ranging from micro(nano)- (<2 nm) to macropores (>50 nm; Figure 7). Similar to battery applications, the cost of the active material used in the electrode is also a limiting factor for SC applications. Usually, AC can be prepared from different organic and biomass precursors through carbonization, which involves heating in the presence of an inert gas followed by selective oxidation of the resulting carbon material by using CO_2, water vapor, or KOH to increase the SSA and PSD. Other factors, such as the time and temperature of the activation step, have a role in fixing the PSD. Gener-

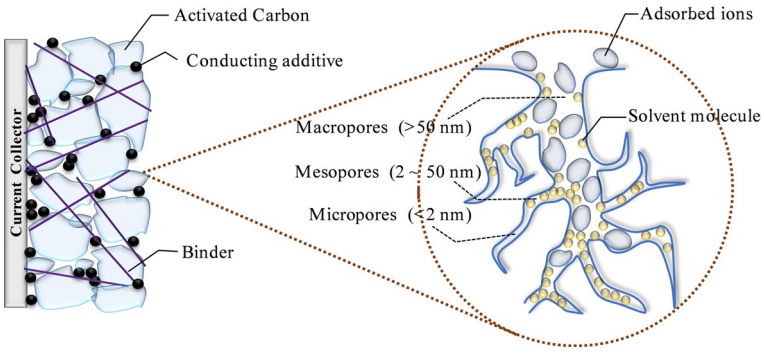

Figure 7. The sizes of different pores presents in carbon materials: micro-, meso-, and macropores.

ally, the specific capacitance of carbon-based EDLCs can attain a value of 100–120 $F g^{-1}$ in an organic electrolyte and can reach up to 150–300 $F g^{-1}$ in the presence of an aqueous electrolyte. However, the operating voltage window is limited in an aqueous electrolyte due to the water-splitting reaction. A typical rectangular-shaped CV curve and linear time–potential curve are characteristic for pure double-layer capacitance.[101]

The capacitive mechanism in ACs is purely based on the physical adsorption or desorption of ions present in the electrolyte into the pores of AC. The required pore size of AC also varies, depending on the choice of electrolyte. For example, AC with a pore size of 0.8 nm is suitable for organic electrolytes, whereas, in the case of aqueous electrolytes, a smaller pore size of 0.4–0.7 nm is preferred.[15] It is very important to control the PSD of AC to attain the maximum value for the energy and power density of an EDLC. The maximum value of capacitance can be obtained if the size of the pores in AC and ions in the electrolyte are equal.[15,102] The industrial production of AC has a long history, but controlling the porosity of AC still remains a difficult task.[103] Commercial AC can offer a specific capacitance of 70–200 $F g^{-1}$ in aqueous electrolytes. However, AC produced by using different activation processes can possess a wide PSD. Moderate activation can also produce AC with a large pore volume and large surface area. Ba et al. developed a low-cost carbon electrode material,[71] which exhibited excellent surface area and high porosity with an organized pore structure of micro-, *meso*- and macropores,[104] after chemical activation by using fig waste as a biomass precursor. These studies have shown that the electrical performance of ACs, including ACs prepared from different biomass waste materials, such as sugarcane bagasse, cellulose, sawdust, and corn grains, is higher than that of other carbon-based nanostructures, such as CNTs and graphene.[104] It is also important to optimize the surface functionality of ACs, which can affect the wettability of the electrode surface; this could also be a reason for the additional increase in capacitance.[104] Other carbonaceous materials, such as CNTs, which are carbon allotropes with cylindrical 1D structures, have received much attention as a SC electrode material on account of their low weight, large surface area, and high electrical conductivity. Remarkably, active particle surfaces prepared by using nanotubes are more effective than those of AC due to their excellent electrochemical performance, such as high specific capacitance and stability under a high current loading, which make them suitable for SC electrode preparation. Chemical vapor deposition (CVD), laser ablation, arc discharge, and high-pressure disproportionation are methods commonly used for the large-scale production of CNTs.[103] As their performance is affected by PSD and internal resistance. Therefore, recent studies have focused on developing flexible carbon fiber (CF) hybrid electrodes.[104] Graphene is another fascinating allotrope of carbon with high thermal and electrical conductivity, large surface area, and high mechanical and chemical stability that is worth mentioning.[103]

Different porous templates can be used for the synthesis of carbon materials with suitable distributions of meso- and macropores. Activation is another method used to control porosity, which can increase micropore distribution. Selection of the carbon precursor has a role in the porosity of the electrode material, which can influence its overall performance. The factors that need to be considered when selecting a carbon precursor for use as an electrode material include availability; cost; the presence of heteroatoms, such as N, B, and P; and the degree of graphitization.[34] Most commercial carbon materials are produced from fossil fuel based precursors (petroleum and coal), which makes them expensive and harmful to the environment. Other problems related to conventional nanostructured electrode materials include high price, low production rate, and difficulty in heteroatom doping.[78] In recent years, research interest has been aimed toward finding suitable green carbon precursors, such as biomass, which is cheaper, abundant, readily available, and renewable. In addition, biomass-based carbon precursors are environmentally friendly and available with porous structures, which has lead researchers to explore their energy-storage applications.[105]

6. Why Use Biomass-Derived Carbon?

Biomass is a renewable energy source that is naturally abundant. Biomass mainly refers to any organic matter, including waste material derived from plants or animals. It is the oldest source of energy after the sun. Biomass is plant matter produced through photosynthesis, in which CO_2 and water from the environment are converted by solar energy into carbohydrates that constitute the plant body. Animals that feed on plants or any other small animals produce biomass, which can be considered as organic waste. Energy from sunlight is stored as chemical energy in biomass and this energy can be widely used to meet our increasing energy needs, such as heating, cooking, and transport fuel. BDC (green carbon) can be produced from different biomass precursors through carbonization and a subsequent activation process.[106] The pyrolysis of various biomass precursors at high temperature under an inert gas leads to the formation of a porous carbon skeleton. In addition, the activation process yields highly interconnected 3D structures with excellent conductivity and tailored porosity, which makes them suitable for various energy-storage applications, mainly in SCs. BDC materials with hierarchical porous structures, periodic patterns, specific nanoarchitectures, controlled morphologies, and modified surface chemistry can be derived from naturally abundant biomass materials. Among all electrode materials available, BDC materials are preferred due to their low ash content, low cost, facile processing techniques, stability, versatile morphology, and mechanical properties.[16,52,54,71,88,89,99,107–112]

Similar to other carbon materials, BDC stores charge through an electrical double-layer mechanism and generally forms EDLC-type SCs. To make a perfect EDLC electrode, the BDC material should have the following properties: 1) large surface area and suitable PSD that corresponds to a large specific capacitance, which ensures high energy and power density of the device; 2) low ESR to ensure a minimal voltage drop in the device; and 3) high stability to ensure good cyclability and long working life.[78] BDC materials have a wide range of appli-

cations, including in energy-storage devices, but the challenge of optimizing their structure or surface properties still needs further research. The electrochemical performance of different BDC materials depends on the capacitance, morphology, and method used to prepare them. Selection of a suitable BDC precursor depends on its cost, intrinsic microstructure, and elemental composition.[112] Different biomass precursors have been selected based on these different criteria; rice straw,[113] wheat straw,[114] popular catkins,[115] and pistachio[116] have been selected due to their low cost and ease of availability. In addition, chicken eggshells[117] and orange peel[118] are examples of precursors that were considered based on their unique hierarchical porous microstructures. At the same time, *Bacillus subtilis*,[90] human hair,[119] and chitin[120] have been selected based on the abundant presence of nitrogen, oxygen, and sulfur atoms in their structures. Both plant and animal waste can be considered as potential carbon precursors for SC electrode materials.[54] In addition, BDC can also be derived from microorganisms, such as fungi (mushrooms and yeasts) and bacterial cellulose,[107,108] which can be considered as good regenerative biomass precursors due to their fast growth rate, richness in nature, and complex chemical compositions.[112]

Generally, volumetric capacitance is used to understand how fast energy can be stored in a unit volume of material. This parameter can be used as an alternative to the gravimetric performance to evaluate the suitability of a biomass precursor for SC applications. Most studies only discuss the gravimetric performance, but, in reality, the volumetric capacity is much more reliable.[78] The volumetric capacitance decreases with an increase in the activation temperature, but it does not match the gravimetric capacitance. The presence of heteroatom-containing functional groups can enhance the volumetric capacitance. Moreover, the use of a three-electrode cell can result in a higher capacitance to that observed by using its two-electrode counterpart.[121] The difference in mass loading, thickness of the electrode, type of binder, and current collector also have some impact on the capacitance. Hence, it is necessary to establish a standard parameter or protocol to accurately determine the capacitance of a device.[54]

Conversion of a biomass precursor into carbon material can be carried out by using carbonization and activation methods. Pyrolysis and HTC are two conventional methods used to carbonize biomass. The pyrolysis of biomass is normally carried out under limited oxygen or inert atmospheres at very high temperatures, whereas HTC involves mixing the carbon precursor with water and then heating the resulting mixture over the temperature range of 150–300 and 300–800 °C for low- and high-temperature HTC, respectively. HTC normally results in the formation of hydrochar with tuned surface chemistry.[110] The preparation of AC can be achieved by using different activation methods, such as physical, chemical, combined physical and chemical, and microwave-induced activation.[105] Recently, several review articles regarding the methods used to convert biomass into BDC have been published.[52,54,99,105,110,112]

Incorporating pseudocapacitance with an EDLC-based biomass-derived electrode can enhance the volumetric capacitance, which can further lead to an increase in energy density. BDC can be modified (composites) by using conducting polymers, transition-metal oxides, or heteroatom doping. This method helps to utilize both electrostatic charges on the carbon material and faradaic reactions on the conducting polymer or transition-metal oxide. The capacitance offered by conducting polymers or transition-metal oxides is higher than that of carbon materials. Nevertheless, carbon materials are more stable and highly conductive compared with pseudocapacitive materials. Nowadays, researchers have incorporated biomass-derived electrodes with pseudocapacitive materials by forming composites or coating them on the surface of the carbon electrode; this can provide high capacitance and stability.[52]

In addition, symmetric SCs fabricated by using a biomass-derived electrode can exhibit low energy density due to their narrow operating voltage window. The only possible route to attain an energy density of 5–10 $Wh\,kg^{-1}$ in a symmetric system is to use an organic electrolyte. To solve this issue, ASCs can be fabricated by using biomass-derived electrodes in combination with a pseudocapacitive or faradaic electrode system. This approach can widen the potential window and help to increase the energy density by combining the two charge-storage mechanisms.

7. ASCs with Biomass-Derived Electrodes

The development of ASCs with a faradaic/pseudocapacitive positive electrode and a capacitive negative electrode is a promising strategy to enhance the overall performance of SCs.[122] These devices normally provide high power density and a wide potential window. The relatively low energy density of ASCs is a major challenge, which needs immediate attention.[78] The formation of ASCs by using conventional nanostructured electrode materials is also associated with other problems, such as high cost, low rate of production, difficulties in heteroatom doping, and the formation of environmentally harmful byproducts.[31,78] These problems can be avoided or eliminated, to some extent, by employing biomass-derived/green carbon sources containing naturally hierarchical structures. Waste materials derived from nature are also a good choice for engineering electrode materials for use in SCs, which, in turn, provide an efficient method for waste management.[122] Recently, ASCs prepared with biomass-derived electrodes have been intensively studied to achieve low-cost ASCs with good energy density. This review gives a comprehensive summary of recent research based on biomass-derived ASCs and their performance.

The energy density of EDLCs based on porous carbon electrodes is limited, but can be overcome by fabricating capacitive ASCs that combine a carbon electrode with a pseudocapacitive electrode. Integrating pseudocapacitive material into the carbon electrode aids mass transport and imparts electrochemical benefits, as a result of the combined action between electrode materials. Among the diverse range of pseudocapacitive materials available, MnO_2 has become known as the most attractive positive electrode candidate in ASCs. MnO_2 can replace expensive RuO_2 due to its abundance, large theoretical capacitance, and low cost.[25,123–125] These benefits are the reasons

behind choosing MnO_2 as the supporting material in composite formation. However, MnO_2 displays low electrical conductivity (10^{-5}–10^{-6} S cm^{-1}), which limits its application in high power and energy density devices. Hence, making a composite from MnO_2 and carbon allows easy access to ions, high conductivity, large surface area, and reduced charge diffusion distances. In recent years, several capacitive ASCs have been developed by using BDC as a negative electrode and MnO_2 as the positive electrode material.[57,126–131] The specific capacitance of these different electrode materials is generally lower than that of the positive electrode material used.[132]

7.1. Bacterial cellulose pellicles

An abundant and low-cost bacterial cellulose-based composite electrode (nitrogen-doped carbonized bacterial cellulose@nickel cobalt layered double hydroxide (CBC-N@LDH)) was prepared by Lai et al.[133] At the outset, raw bacterial cellulose (BC) pellicles were freeze-dried in liquid nitrogen and then immersed into a solution of HCl containing aniline monomers to accomplish an oxidative polymerization process to form polyaniline through the addition of ammonium persulfate. Thus, the as-obtained N-doped polyaniline-coated BC nanofibers (N-CBC) were freeze-dried and carbonized at 700 °C under an argon atmosphere and utilized in the synthesis of the Ni–Co layered double hydroxide (LDH) composite. N-CBC shows a high specific capacitance of 238 F g^{-1} at a current density of 0.5 A g^{-1}. For this synthesis, a solution codeposition method was used by employing a solution of metal nitrate with N-CBC at 80 °C for 8 h. The resulting composite possessed a high surface area of 405.8 m^2 g^{-1} with pore sizes in the range of 1–10 nm. At a current density of 1 A g^{-1}, the composite showed a specific capacitance of 1950 F g^{-1}. Furthermore, this porous material was used in an ASC as the positive electrode (CBC-N@LDH), along with a N-CBC negative electrode, which showed a notable capacitance of 63.8 F g^{-1} at 10 A g^{-1} and operated over a wide potential window of 0–1.6 V. Its good electrochemical performance was further confirmed by an energy density of 36.3 Wh kg^{-1} at 0.8 kW kg^{-1}, which showed a slight decrease (22.7 Wh kg^{-1}) at a high power density of 8 kW kg^{-1}. This performance was mainly attributed to the good conducting nature of the N-doped carbon nanofibers, as well as the unique structure of Ni–Co LDH. The authors reported that the assembled ASC exhibited 89.3% capacitance retention, even after 2500 cycles.

In another study, Shan et al. effectively utilized BC as a source of carbon material for the synthesis of 3D honeycomb-like hierarchical structured carbon (HSC).[134] BC pieces were frozen in liquid N_2 and the resulting aerogel was immersed into a solution of KOH at different concentrations (0.05, 0.1, 0.2, and 0.5), for 12 h at room temperature. Furthermore, the KOH-activated materials were again subjected to freeze-drying at −50 °C followed by pyrolysis at 700 °C for 2 h under an N_2 atmosphere to give HSC-*x* (*x* = concentration of KOH; Figure 8). The authors explained that KOH performed three functions during the activation process: 1) KOH helps to cross-link BC, transforming the structure of BC from nanofibers to nanosheets; 2) KOH acts as a hard template to generate macropores (ion buffering reservoirs), which effectively reduce the diffusion pathway of the electrolyte ions; and 3) KOH functions as a chemical activating agent to generate macropores by eroding the carbon structure. Thus, $HSC_{0.2}$ exhibited a large SSA of 1533 cm^2 g^{-1} and a specific capacitance of 422 F g^{-1} by using a 6 M KOH as the electrolyte. Additionally, Ni–Co–Al layered double hydroxide (Ni-Co-Al LDH) was synthesized through a urea-assisted solvothermal process under hydrothermal conditions at 150 °C for 12 h, which showed a surface area of 96.4 m^2 g^{-1}, along with a mesoporous structure. In a three-electrode system, Ni-Co-Al LDH exhibited a specific capacitance of 1480 F g^{-1} at 2 mV s^{-1} in 6 M KOH. The SSC based on HSC could deliver an energy density of 37.3 Wh kg^{-1} with 1 M Na_2SO_4 electrolyte. If the ASC was assembled by using HSC as the negative electrode and Ni-Co-Al LDH as the positive electrode, the device produced an energy density of 100 Wh kg^{-1} and retained 33 Wh kg^{-1} at a high power density of 36.8 kW kg^{-1}. The ASC showed excellent cycling stability, even after 10000 cycles, with a 13% increase in specific capacitance relative to the initial cycle in 6 M KOH; thus encouraging researchers to fabricate ASCs from BC.

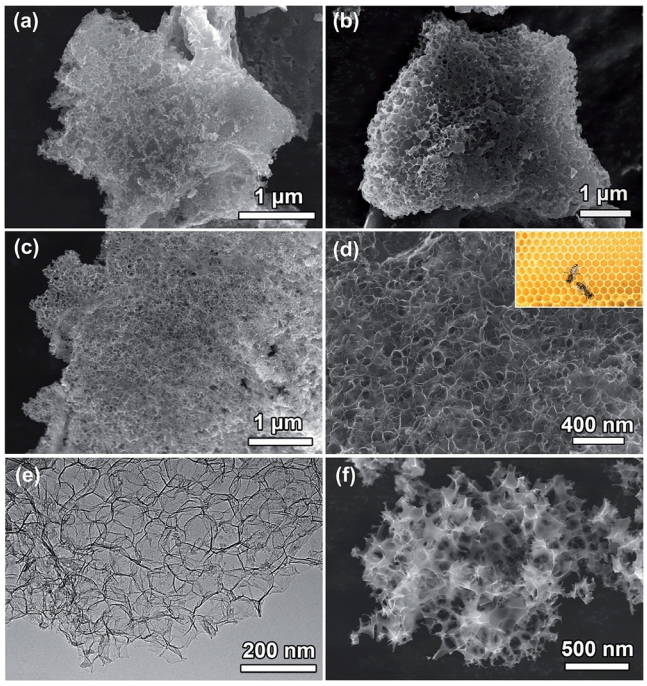

Figure 8. SEM (a–d, f) and TEM (e) images of HSC-0.05 (a), HSC-0.1 (b), HSC-0.2 (c–e), and HSC-0.5 (f). The inset of d) shows the honeycomb morphology (reproduced with permission from Ref. [134]; copyright Royal Society of Chemistry, 2016).

The formation of capacitive ASCs with a BDC electrode and MnO_2-based composite electrode was also studied by Chen et al.[87] The authors developed a green approach to construct a binder-free ASC by using bacterial cellulose-derived carbon nanofibers loaded with MnO_2 as the positive electrode and nitrogen-doped carbon nanofibers as the negative electrode with 1 M Na_2SO_4 electrolyte (Figure 9). In the first step, the abundant resource of p-BC pellicles was calcined at high tem-

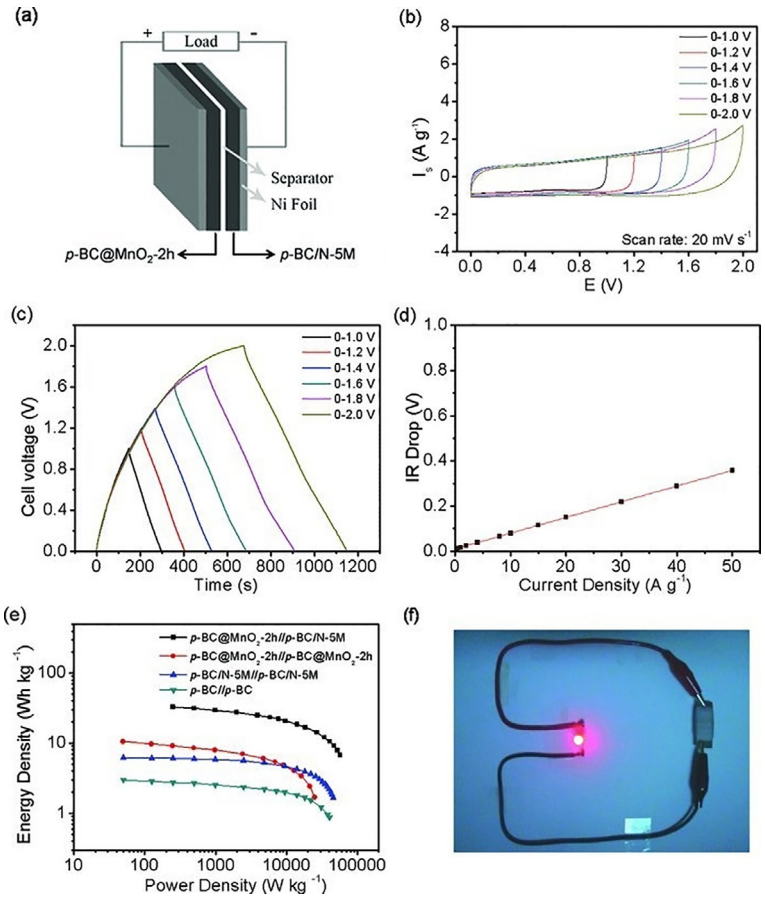

Figure 9. The capacitive performance of the ASC (p-BC@MnO_2-2h/p-BC@N-5M; p-BC = pyrolyzed bacterial cellulose, MnO_2-2h = MnO_2 coated on p-BC in 2 h using 0.1 M $KMnO_4$/0.1 M K_2SO_4 aqueous solution, N-5M = 5.0 M urea aqueous solution) prepared by using p-BC@MnO_2-2h as the positive electrode and p-BC@N-5M as the negative electrode in 1 M Na_2SO_4 aqueous electrolyte. a) A schematic representation of our ASC device. b) CV curves of the different operation voltages obtained at a scan rate of 20 mV s^{-1}. c) GCD curves of different operation voltages obtained at a current density of 0.25 A g^{-1}. d) The potential drop (V_{drop}) obtained at different discharge current densities. e) Ragone plots obtained for the SCs. f) A digital photograph of a red light-emitting diode (LED) powered by using the p-BC@MnO_2-2h/p-BC@N-5M device (reproduced from Ref. [87]; copyright Wiley-VCH, 2014).

perature (1000 °C) under an N_2 atmosphere for 2 h, then dipped into a mixed salt solution of $KMnO_4$ and K_2SO_4 to form the MnO_2-decorated carbon composite (p-BC@MnO_2). The morphology of the as-obtained composite was analyzed by means of SEM, which showed the 3D structure of adjacent nanowires and further clarified the uniform distribution of Mn on the carbon material, whereas calcined p-BC displayed a network structure in the form of 10–20 nm nanowires with several interconnected pores. In the second step, nitrogen-doped p-BC (p-BC@N) was formed by employing urea as a reducing agent under hydrothermal conditions, revealing a high BET surface area of 252.23 $m^2 g^{-1}$ and 3D pellicle structure, which consisted of nanowires and cross-linked pores. The fabricated p-BC@MnO_2 and p-BC@N materials were used as the positive and negative electrodes in an ASC and established an operational voltage window of 2 V in 1 M Na_2SO_4 electrolyte, as well as extraordinary cycling stability after 2000 charge–discharge cycles with 95.4% capacitance retention. In addition, this device can deliver a high energy density of 32.91 Wh kg^{-1}, along with a maximum power density of 0.284 kW kg^{-1}, due to the high working voltage and good capacitance of the two electrodes. A practical application was also carried out by using this prototype ASC device, which involved powering a red LED for 90 s after being charged at 2 V for 44 s (Figure 9).

7.2. Orange peel

The effective utilization of orange peel (waste biomass) to construct a MnO_2-based capacitive ASC was demonstrated by Sun et al. (Figure 10).[127] Orange peel was used to fabricate the electrodes, electrolyte, and separator in the ASC. One-step carbonization of orange peel at 800 °C for 3 h formed a porous powder (OPHPC) with desired size and thickness, which was directly exploited as the negative electrode material in the ASC. Formation of the porous carbon material was attributed to the presence of potassium and calcium atoms, which induced the chemical activation process and the formation of gases, such as CO_2 and H_2, during the calcination step that also acted as activating agents. OPHPC showed a SSA of 860 $m^2 g^{-1}$, which was calculated by using DFT. The natural nitrogen-doped OPHPC was characterized by means of X-ray photoelectron spectroscopy (XPS) analysis, which showed peaks at 403.2, 401.8, 400.3, and 398.6 eV, corresponding to the oxidized, graphitic, pyrrolic, and pyridinic N atoms, respectively. The positive electrode material was prepared by immersing the OPHPC into a pre-prepared solution of $KMnO_4$, which resulted in the formation of the MnO_2 composite under hydrothermal conditions at 180 °C for 1 h. The oxidation state of Mn^{4+} in the composite was analyzed by XPS. The authors developed an all-orange-peel solid-state ASC (Figure 10b) by using OPHPC as the negative electrode, MnO_2-incorporated OPHPC as the positive electrode (MnO_2@OPHPC), a thin orange peel (mesocarp) separator, and gel electrolyte (prepared from orange peel), which presented an areal capacitance of 3987 mF cm^{-2} at a current density of 1 mA cm^{-2}. The presence of alkali ions in the natural electrolyte, including Na^+, K^+, and Mg^{2+}, resulted in an electrical conductivity of 61 S m^{-1}, whereas the gel electrolyte had an electrical conductivity of 45.3 S m^{-1}, which was acceptable for use in ASCs. Based on the electrode and device, the specific capacitance was calculated to be 65 and 27 F g^{-1}, respectively. Furthermore, various forms of the electrodes, including helix, pentagram, annulus, and heart-shaped structures, can be tailored by utilizing orange peel, which can be used to load metal oxides to synthesize various positive electrode materials.

Most recently, Kaippannan and Marappan reported the utilization of orange-peel-derived AC (OPAA) as a negative electrode material in a high-performance ASC stack.[136] Hydrated $Ni(OH)_2$ nanosheets were prepared through the chemical de-

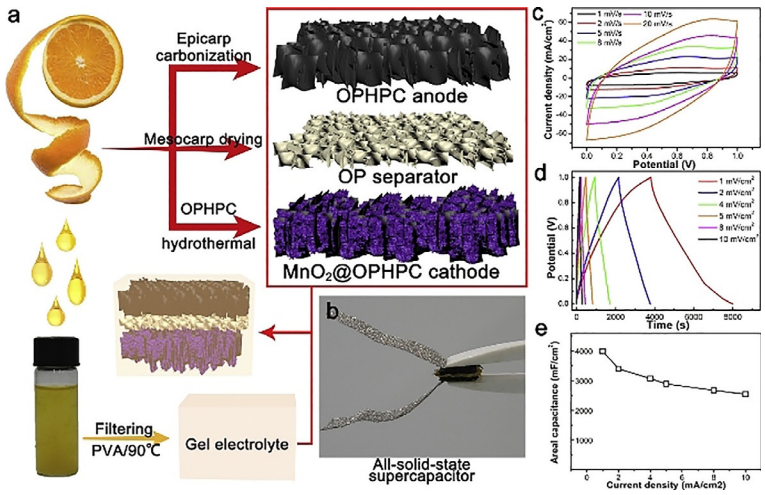

Figure 10. a) A schematic representation of all-solid-state SCs derived from orange peel. PVA = polyvinyl acetate. b) A digital photograph of the resulting all-solid-state SC. c) CV and d) GCD curves obtained for the device, and e) the corresponding areal capacitance (reproduced with permission from Ref. [127]; copyright Elsevier, 2014).

composition of nickel hexacyanoferrate and used as a positive electrode in an ASC. OPAA was prepared through carbonization at 600 °C for 3 h under an argon atmosphere followed by KOH activation in a mass ratio of 1:3. The obtained slurry was further heated to 700 °C at a heating rate of 5 °C min^{-1} and then dried at 80 °C for 5 h to give OPAA-700. The $Ni(OH)_2$ nanosheets used were highly crystalline, with an average crystal size of 10 nm, as observed from XRD analysis. The nitrogen adsorption–desorption isotherms of $Ni(OH)_2$ showed its mesoporous nature, with an average PSD of 3.6–5.7 nm, which could exhibit an SSA of 206 m^2 g^{-1} with a pore volume of 0.270 cm^3 g^{-1}. Moreover, the authors also reported that these nanosheets showed a specific capacity of 1126 C g^{-1} at a current density of 2 A g^{-1}. The authors also stated that, to achieve high-level performance, charge storage in the negative and positive electrodes should be the same; this can be achieved by using an appropriate active material loading. The aqueous ASC fabricated at a mass loading of about 8 mg cm^{-2} on the negative electrode and 2 mg cm^{-2} on the positive electrode exhibited a voltage of 1.6 V. The ASC stack assembly was constructed by using a combination of six cell stacks, which were connected in series, and each cell stack contained six cells in parallel (Figure 11). The full cell assembly shows high energy and power values of 30 mW h^{-1} and 1632 mW, respectively, with good electrochemical stability and 81% capacity retention, even after 100 000 charge–discharge cycles. Furthermore, the assembled ASC device can power 285 white LEDs for more than 3 min; thus revealing its potential application in energy-storage devices.

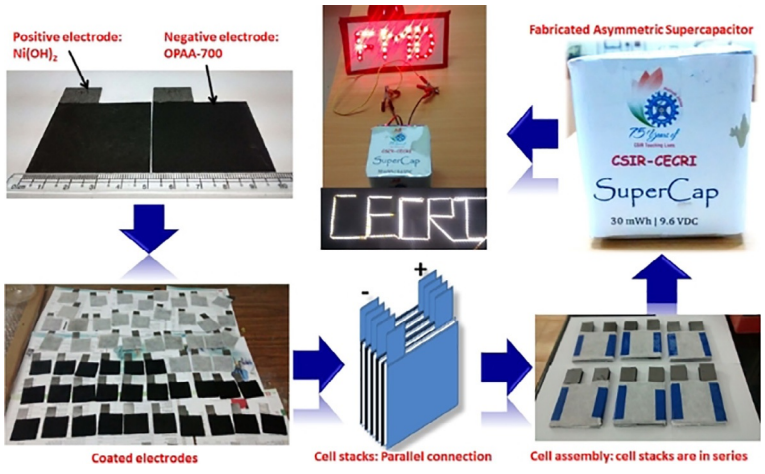

Figure 11. Step-by-step fabrication of an ASC device using orange-peel-derived AC as a negative electrode (reproduced with permission from Ref. [136]; copyright the authors, 2019).

7.3. Willow catkin

Li et al. established the idea for the development of a BDC/metal hydroxide hybrid composite.[89] Furthermore, the authors fabricated an ASC by using porous carbon microtubes (PCMTs) derived from willow catkin biomass as the negative electrode. Willow catkin is a good biomass precursor with a hollow tubular microstructure, which can serve as a biotemplate to prepare a carbon matrix used to support active nanomaterials. The authors prepared a composite of β-$Ni(OH)_2$ nanosheet arrays anchored on willow catkin derived hollow carbon microtubes (ACMTs) through an acid treatment and hydrothermal process. Briefly, willow catkins were carbonized under an argon atmosphere and the resulting powder was oxidized with HNO_3 to attain a hydrophilic surface. Then, the β-$Ni(OH)_2$-ACMT composite was prepared under hydrothermal conditions through urea hydrolysis at 150 °C for 6 h. The freeze-dried product had a surface area of 155.7 m^2 g^{-1}, and TEM analysis revealed its hollow tube structure with diameters in the range of 6–10 μm and a wall thickness of 200–400 nm (Figure 12). The uniform growth of β-$Ni(OH)_2$ nanosheets with a thickness of 30 nm on both the external and internal surfaces of the ACMT were observed (Figure 12 d,e), which produced ample active sites for the redox reaction. The ASC prepared by using the β-$Ni(OH)_2$@ACMT composite as a positive electrode and PCMT as the negative electrode in 6 M KOH retained 43.8% of its initial capacitance at a high current density of 20 A g^{-1}, and could achieve a high energy value of 37.8 W h kg^{-1} at a power density of 0.75 kW kg^{-1}. The cycling performance also implied that this ASC device had the capability to drive up to 3000 cycles at 5 A g^{-1} with 80.8% capacitance retention.

In another study utilizing willow catkin as biomass waste, Li et al. reported anchoring of MnO_2 nanoplates on biomass-derived cross-linked carbon nanosheets (CCNs) through a two-step procedure.[57] Initially, seeds of willow catkin were removed, transferred into a solution of KOH, and heated at 100 °C to remove residual water. The resultant mixture was further heated under an argon atmosphere at 400 °C

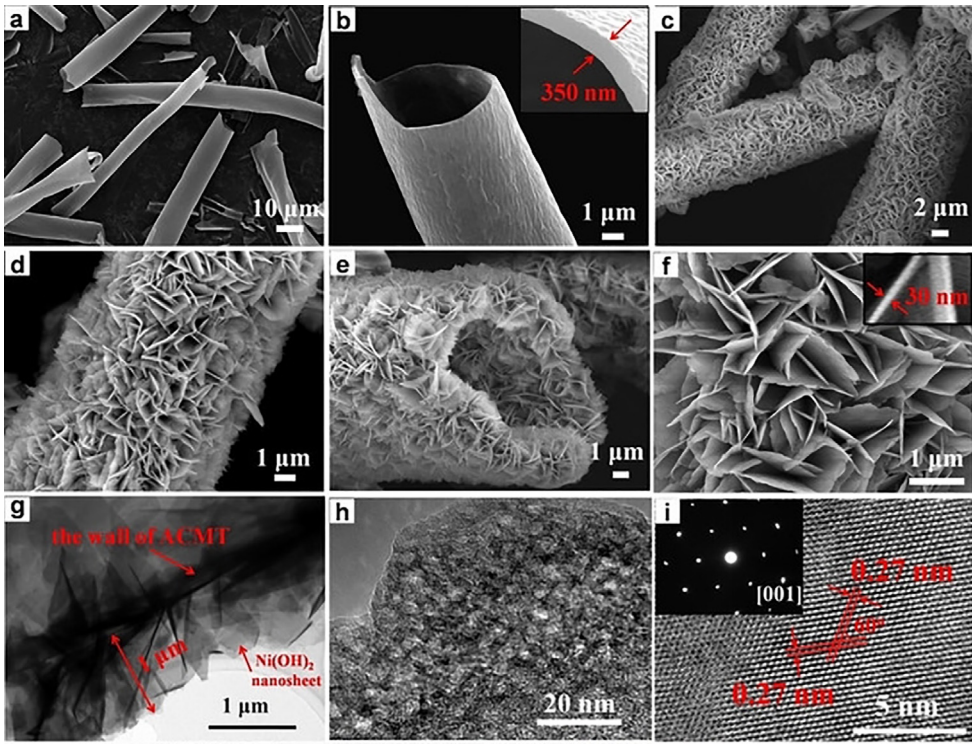

Figure 12. SEM images of ACMT (a,b) and β-$Ni(OH)_2$@ACMT (c–f) at different magnifications. g) TEM image of β-$Ni(OH)_2$@ACMT. TEM (h) and high-resolution (HR) TEM (i) images of an individual $Ni(OH)_2$ nanosheet. The inset is the corresponding selected-area electron diffraction (SAED) pattern of an individual $Ni(OH)_2$ nanosheet (reproduced from Ref. [89]; copyright Wiley-VCH, 2018).

for 3 h. To synthesize the CCNs, the calcination step was continued under the same atmosphere, increasing the temperature to 850 °C for 1 h, which resulted in a high surface area of 1507 $m^2 g^{-1}$. In the second step, MnO_2 was deposited onto the CCNs to form the composite through an in situ hydrothermal reaction, which resulted in a surface area of 234 $m^2 g^{-1}$. The interconnected thin carbon nanosheets prepared from willow catkin interact with MnO_2 through its 3D cross-linked structure, wherein it can offer conducted networks for electron transport. The amorphous nature of MnO_2 was observed in the XRD spectra, which displayed broad peaks and the α-MnO_2 plane, whereas the diffraction peak at about 25° corresponded to the (002) plane detected for the CCNs. For further confirmation, the existence of Mn was estimated in the composite through XPS analysis. A capacitive ASC was constructed by using CCNs as the negative electrode and MnO_2@CCNs as the positive electrode in 1 M Na_2SO_4 electrolyte, which demonstrated a specific capacitance of 47 $F g^{-1}$ at 0.2 $A g^{-1}$ after showing individual performances of 141 and 188 $F g^{-1}$, respectively. Moreover, the ASC lost only 1.4% of its initial capacitance at 1 $A g^{-1}$, even after 10000 cycles, which indicated its excellent cycling stability. Additionally, this promising device can deliver an energy density of 23.6 $Wh kg^{-1}$ at a power density of 0.19 $kW kg^{-1}$, which is suitable for application in portable electronic devices.

7.4. Pine cone

Barzegar et al. studied the possibility of developing an ASC device from two different carbon materials (i.e., activated expanded graphite (AEG) and pine cone activated carbon (PAC)),[137] which had the same electrostatic charge-storage mechanism (EDLC) in both electrodes.[138] The authors used naturally abundant pine cone biomass as a carbon source and prepared PAC through KOH activation followed by carbonization in the presence of Ar and H_2 at 800 °C for 2 h with a KOH/PAC ratio of 4:1. AEG was obtained by expanding graphite in a microwave oven, which was subsequently dispersed in polyvinylpyrrolidone, mixed with KOH, and then carbonized at 800 °C for 2 h under a mixture of gases. The authors formed an ASC by using AEG and PAC as the positive and negative electrodes, respectively; this maintained SSAs of 457 and 808 $m^2 g^{-1}$, respectively. This device showed a specific capacitance of 277 $F g^{-1}$ at 0.5 $A g^{-1}$ and an energy density of 24.6 $Wh kg^{-1}$ at a power density of 0.4 $kW kg^{-1}$. It also exhibited good stability when subjected to a floating test for 110 h and a safe operational voltage window of 1.6 V in a gel electrolyte.

7.5. Hemp stems

Yang et al. reported the incorporation of MnO_2 into 3D honeycomb-like AC (3D HC), which was derived from hemp biowaste through carbonization at 600 °C followed by steam activation at 800 °C for 2 h.[126] The as-formed carbon material has a 3D honeycomb structure with interconnected pores in the range of 5–60 μm, which can act as a substrate; thus allowing the deposition of an electroactive material onto its structure. Under hydrothermal conditions at 140 °C for 24 h, MnO_2 nano-

wires were grown on the porous structure of HC, resulting in the formation of a 3D MnO_2@HC composite by using a mixed solution of $MnSO_4$ and $KMnO_4$. A large surface area of 438 $m^2 g^{-1}$ was obtained for the composite, whereas the surface area of HC was only 238 $m^2 g^{-1}$, as a result of the growth of MnO_2 nanowires in the 3D HC pores during the hydrothermal reaction. Furthermore, the authors stated that the MnO_2@HC composite was a promising electrode material for SC applications because it displayed a high specific capacitance of 340 $F g^{-1}$ at 1 $A g^{-1}$, whereas 3D HC acquired only 168 $F g^{-1}$. The ASC fabricated by using HC as the negative electrode and 3D MnO_2@HC as the positive electrode in 1 M Na_2SO_4 electrolyte lost only 2% of its initial capacitance over 3000 cycles, and provided a maximum energy and power density of 33.3 $Wh kg^{-1}$ and 14.8 $kW kg^{-1}$, respectively. This admirable electrochemical performance was achieved by using the features of MnO_2 wires, the structural integrity and quick ion/electron transfer exhibited by the macroporous structure of HC, and low ohmic loss observed during the course of the charging–discharging process.

7.6. Tofu

Low-dimensional materials, especially 1D nanostructures, have large ion-accessible surface areas, excellent mechanical stability, and rapid electron transport pathways, which make them the most suitable candidates for high-performance SCs. Ouyang et al. reported a stripping and cutting strategy to form N-doped porous 1D carbon nanobelts (CNBs) through cooking tofu biomass in $ZnCl_2$ molten salt.[128] The benefit of synthesizing carbon materials with molten salts as the reaction media is that the homogeneous ionic-liquid medium has high polarity, which promotes the carbonization process.[139,140] This method has already been used for the synthesis of other carbon nanomaterials, including nanodiamonds,[141] nanosheets,[142] and graphene.[131] This is a simple, economic, and scalable method, in which the molten salt can be recycled. In this study, molten $ZnCl_2$ salt and tofu powder, which was frozen in liquid nitrogen, were mixed uniformly in a 10:1 ratio for pyrolysis at different temperatures under an argon atmosphere to produce 1D CNBs. This technique gave a high carbon yield (≈20%), unlike other chemical activation processes, because of the absence of any chemical reaction between $ZnCl_2$ and C during the course of the carbonization process. The intercalation of $ZnCl_2$ triggered the conversion of bulk tofu particles into carbon nanosheets through continuous exfoliation. In addition, the pores present in the carbon material were fully occupied with Zn^{2+} ions, which instigated the lengthwise cutting effect. Finally, the self-assembly process occurring in the $ZnCl_2$ molten salt formed 1D CNBs with lengths of 3–5 μm without the need for any chemical reagents and equipment; this was proven by SEM analysis. Raman spectroscopy was used to evaluate the degree of graphitization in the as-obtained amorphous carbon material, which possessed a large surface area of 1208 $m^2 g^{-1}$ and a total pore volume of 1.381 $m^2 g^{-1}$. Furthermore, the CNBs were transferred into a solution of $KMnO_4$ to form a MnO_2@CNBs composite through in situ hydrothermal deposition at 120 °C for 1 h; the presence of all elements in the material was confirmed by XPS analysis. The composite showed a BET surface area of 68.4 $m^2 g^{-1}$, which exhibited a type IV isotherm with an H4 hysteresis loop. Notably, the CNB/MnO_2@CNB-based ASC, with 1 M Na_2SO_4 electrolyte, exhibited a specific capacitance of 54 $F g^{-1}$ at 0.5 $A g^{-1}$ and could deliver an energy density of 24.29 $Wh kg^{-1}$ at a power density of 0.49 $kW kg^{-1}$. Moreover, this device has the power to drive 10000 cycles at 3 $A g^{-1}$; thus retaining 95.8% of its initial capacitance, which was attributed to the structure of the 1D CNBs improving electron transport and decreasing the number of ion-diffusion pathways.

7.7. Natural basswood blocks

Chen et al. successfully demonstrated the novel design concept of an all-wood-structured ASC utilizing activated wood carbon (AWC) as the negative electrode, a thin wood membrane as the separator, and MnO_2/wood carbon (MnO_2@WC) as the positive electrode (Figure 13).[129] The natural basswood blocks were sliced to a preferred thickness for carbonization at 1000 °C under an argon atmosphere for 6 h after stabilization at 250 °C. In this study, CO_2 activation was used to activate carbonized wood at 750 °C for 16 h, creating numerous nanopores. Raman spectroscopy and HRTEM analysis of the AWC unveiled the amorphous nature of this hard carbon material with disordered domains. The positive MnO_2@WC electrode was prepared through electrodeposition of Mn onto the wood-derived carbon through an anodizing method. The homogeneous distribution of MnO_2 nanosheets on both inside and outside of the WC channels was detected by means of TEM analysis. Due to the presence of numerous open channels in this natural wood material, the assembled ASC showed low tortuosity. At the same time, factors such as large thickness, high mass loading, high conductivity, and hierarchical pore structure of the electrode material result in high areal capacitance and rate capability values. A maximum specific capacitance of 24.1 $F g^{-1}$ reflected the MnO_2@WC rate capability at a high current density of 30 $mA cm^{-2}$, whereas the AWC electrode could maintain 104 $F g^{-1}$ at the same current density. The all-wood-structured ASC exhibited an aerial capacitance of 3.6 $F cm^{-2}$ (≈35.6 $F g^{-1}$ based on the total mass of the electrode materials) at a current density of 1 $mA cm^{-2}$. The assembled ASC also demonstrated a maximum energy density of 16 $Wh kg^{-1}$ at a power density of 0.005 $kW kg^{-1}$ and 93% of its initial capacitance could be retained, even after a long lifetime of 10000 cycles, with a gel electrolyte prepared from PVA/LiCl. Thus, this design was a great success because it was a low cost, high mass loading, nondeformable, and biocompatible SC for green and renewable energy storage.

7.8. Loofah sponge

A novel ASC, which was operable in a neutral electrolyte and prepared by using loofah sponge as the source of carbon material, was developed by Luan et al.[130] Loofah sponges were ground, carbonized at 600 °C, mixed with KOH in a 1:2 ratio,

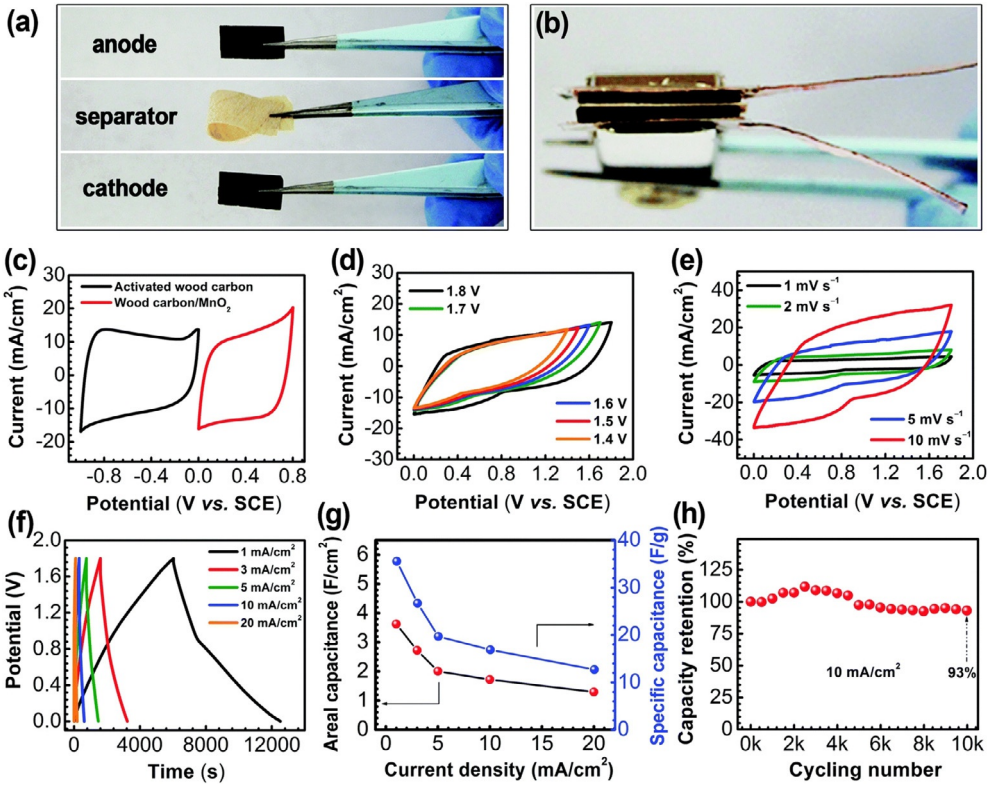

Figure 13. a) Photographs of the AWC anode, wood separator, and MnO_2@WC cathode. b) Photograph of the all-wood-structured all-solid-state ASC. c)–h) The electrochemical performance of the AWC//wood separator//MnO_2@WC ASC. c) Typical CV curves obtained for the AWC anode and MnO_2@WC cathode over the potential range of −1 to 0.8 V. CV curves obtained over d) different potential ranges and e) various scan rates. Charge–discharge profiles at different f) current densities, g) rate performances, and h) cycling performance. The specific capacitance values were calculated based on the total mass of both electrodes (reproduced with permission from Ref. [129]; copyright Royal Society of Chemistry, 2017).

and subjected to pyrolysis at 800 °C for 1 h under an argon atmosphere. The pyrolyzed material (LS-C) was further washed with HCl to remove impurities and a composite formed with MnO_2. The hydrothermal reaction was performed to decorate the BDC material on MnO_2 (LS-C@MnO_2) at 140 °C, as a result of employing $KMnO_4$ in HCl. SEM images confirmed the uniform growth of MnO_2 rodlike structures on the LS-C. MnO_2 cross-linked nanorods with diameters of 80–100 nm and lengths of 3–5 μm were observed by using TEM. Additionally, nitrogen-doped LS-C was prepared through a urea-assisted hydrothermal reaction at 180 °C for 10 h. Large surface areas of 1747 and 759 $m^2 g^{-1}$ were observed for LS-C and LS@MnO_2, respectively; thus resulting in more reactive sites for electrochemical reactions to take place, which is beneficial for attaining a high-performance energy device. The ASC was formed by using N-doped porous carbon (LS-C) as the negative electrode and MnO_2-incorporated porous carbon (PC@MnO_2) as the positive electrode. The designed ASC can achieve a working voltage of 1.8 V and a specific capacitance of 78 $F g^{-1}$ at a current density of 1 $A g^{-1}$. The energy and power density values were 34.7 $Wh kg^{-1}$ and 26.8 $kW kg^{-1}$, respectively. Moreover, the device can retain 91.2% of its initial specific capacitance after 2000 cycles at 1 $A g^{-1}$; thus exhibiting 71.4% capacitance.

7.9. Eggplant

Transition-metal oxides and sulfides have been widely used as the positive electrode material in ASCs due to their high pseudocapacitance.[56,143,144] Among them, MnS nanocrystals have attained great importance because of their high electric conductivity, large theoretical capacitance, and low cost. MnS is a direct p-type semiconductor with a wide band gap (3.1–3.7 eV), which exists in three different crystallographic phases (α, β, and γ forms). Wurtzite-type γ-MnS has edge-sharing Mn octahedra and a laminar structure, which enhances the intrinsic electrochemical reactivity for capacitive behavior. By assembling novel γ-MnS nanocrystals as the positive electrode, Chen et al. developed an all-solid-state ASC with eggplant-derived activated carbon (EDAC) as the negative electrode in an agar gel solid electrolyte.[145] The eggplant powder was subjected to heating at 300 °C under an argon atmosphere in the initial process and mixed with KOH in a 1:2 mass ratio. The as-prepared material was calcined at 700 °C under an argon atmosphere for 4 h through vapor deposition polymerization followed by sonication with HNO_3 as the activation step. KOH activation changes the nonporous structure of eggplant into a porous honeycomb-like structure, along with several crossed holes, which were detected through field-emission (FE) SEM and TEM analyses. The PSD in EDAC was examined by means of nitrogen adsorption–desorption analysis, which revealed a large

BET surface area of 2764.3 $m^2 g^{-1}$ with a total pore volume of 1.09 $cm^3 g^{-1}$, as well as mesoporous flags (>2 nm) that achieved 396 $F g^{-1}$ at 0.5 $A g^{-1}$. The high BET SSA, microporous area, and pore volume of the EDAC can promote the reversible adsorption or desorption of electrolyte ions on the surface of the carbonaceous material, which increases the energy density of the ASC. The assembled MnS/EDAC asymmetric device exhibits a specific capacitance of 110.4 $F g^{-1}$ at a current density of 0.5 $A g^{-1}$ after 5000 cycles, and the device can retain 89.87% of its initial capacitance. It also showed an energy density of 37.6 $Wh kg^{-1}$ and a power density of 0.18 $kW kg^{-1}$. A practical application was demonstrated by connecting two ASCs in series to power a red LED for 15 min.

7.10. Bamboo leaves

Bamboo is a naturally abundant, silicon-accumulating plant. The cultivation of bamboo produces a large number of waste bamboo leaves, which contain nearly 17–23 wt% silica.[146] Pyrolysis of bamboo leaves produces porous carbon with inherent silicon atoms. Wang et al. presented a method of converting natural bamboo-leaf-derived porous carbon into manganese silicate carbon material (MnSi-C) and reported its application in ASCs.[147] Dried bamboo leaves were carbonized at 600 °C to form micropores in the sample to help increase the overall electrochemical performance. The resultant material, SiO_2-C, had a composition of 76.7 wt% carbon and 23.3 wt% SiO_2, which was determined by means of inductively coupled plasma atomic emission spectroscopy (ICP-AES) analysis. Furthermore, a hydrothermal reaction helped to decorate manganese silicate on the resultant carbon material by reacting added manganese ions with the inherent silicon species present in the carbon material at 180 °C for 24 h. The bamboo-leaf-derived MnSi-C displayed a high SSA of 300.3 $m^2 g^{-1}$ with a total pore volume of 0.354 $cm^3 g^{-1}$. In addition, functional groups such as –N=, –NH–, =S, $–SO_x$, –SH, and $–SiO_4$, were identified through FTIR spectroscopy and XPS analyses. The single electrode constructed from MnSi-C exhibited a capacitance of 162.2 $F g^{-1}$ at a current density of 0.5 $A g^{-1}$, and 85% of its initial capacitance was retained after 10000 charge–discharge cycles in 3 M KOH. The authors also assembled an ASC by using MnSi-C as the negative electrode, $Ni(OH)_2$ as the positive electrode, and PVA/KOH electrolyte, which exhibited a specific capacitance of 438.5 $mF cm^{-2}$ at 4 $mA cm^{-2}$ and delivered a maximum energy density of 24.6 $Wh kg^{-1}$ and power density of 0.6 $kW kg^{-1}$. However, this device failed to attain good cycling stability, retaining only 34% of its initial capacitance after 1000 cycles at a current density of 1 $A g^{-1}$.

7.11. Banana fibers

During the process of finding new electrode materials for high-performance SCs, Chaitra et al.[148] reported the use of porous carbon material derived from banana fibers for SC electrode applications.[18] Banana fibers were carbonized under an N_2 atmosphere and then mixed in a 1:4 ratio with a 10 M solution of KOH. The activated material was heated at 750 °C under N_2 for 1 h to form the (002) and (100) planes of graphite, which was confirmed by means of XRD analysis. Raman spectroscopy also confirmed the presence of an increased number of defects after the KOH activation process, in the form of defective carbon crystallites and crystalline graphene peaks, corresponding to the D and G bands, respectively. The surface area increased from 4.1 to 957 $m^2 g^{-1}$ after the untreated carbon material was activated with KOH, and displayed a type IV isotherm with H3 hysteresis loop; thus confirming its mesoporous nature. In addition, the hollow carbon cavities present in the BDC were anticipated to enhance the overall charge-storage capacity of the device by permitting the electrolyte ions to enter easily; thus decreasing the ESR. As expected, the banana-fiber-derived carbon material displayed a high specific capacitance of 324 $F g^{-1}$, whereas the untreated carbon material achieved only 131 $F g^{-1}$ at 10 $mV s^{-1}$ in 1 M KOH electrolyte. Subsequently, the authors designed an ASC device by using KOH-activated porous carbon material derived from banana fibers as a negative electrode and β-$Ni(OH)_2$@MWCNTs[149] as the positive electrode. If 1 M KOH was used as the electrolyte, the device showed a wide operational voltage window of 2.2 V and superior electrochemical performance, such as a high energy density of 63 $Wh kg^{-1}$ and a power density of 1 $kW kg^{-1}$, due to the unique structures of the electrode materials. Moreover, an outstanding cycling performance of 5000 cycles was achieved for this device, even at a high current density of 25 $A g^{-1}$, with 100% capacity retention. This ASC device was constructed from cheap BDC materials and could power different colors of LEDs and a minifan.

7.12. Pomelo fruit

Qu et al. also presented the fabrication of an ASC based on BDC.[150] The authors used the peel of pomelo fruit as a carbon source, ammonia as a dopant, and KOH as an activating agent to produce porous framework-like N-doped carbon (PFNC) material. The recovered pomelo peel was initially carbonized under hydrothermal conditions followed by calcination at 300 °C. Subsequently, the material was mixed with KOH in a 1:3 ratio, transferred to a graphite crucible, and heated at 800 °C for 2 h under a nitrogen atmosphere to yield porous framework-like carbon without any dopant (PFC), which displayed bands at 1350 and 1580 cm^{-1} in its Raman spectrum. The presence of sp^3-hybridized carbon atoms in the resultant PFC was attributed to disordered carbon, which corresponded to the band observed at 1350 cm^{-1}, whereas the in-plane vibrations due to sp^2-hybridized carbon atoms were observed at 1580 cm^{-1}. The PFC material was further treated with 10% NH_3 under hydrothermal conditions by using the same procedure to form PFNC, which exhibited a large surface area of 1648.6 $m^2 g^{-1}$ and a total pore volume of 0.8925 $cm^3 g^{-1}$. The assembly exhibited a remarkable specific capacitance of 260 $F g^{-1}$, whereas the PFC material showed a specific capacitance of only 230 $F g^{-1}$ at 1 $A g^{-1}$ in 2 M KOH electrolyte. The authors also made hierarchical porous flake-like NiO arrays on the surface of Ni foam (PFN), which served as the positive electrode of an ASC assembled with PFNC as the negative elec-

trode. The PFN/PFNC device exhibited a high specific capacitance of 88.8 $F g^{-1}$ at 0.4 $A g^{-1}$ and an energy density of 27.75 $Wh kg^{-1}$ at 0.3 $kW kg^{-1}$. The device also demonstrated superior cyclic performance over 5000 cycles, with an outstanding initial capacitance retention of 80.2%. Two PFN/PFNC ASC assembled in series were able to power two red LEDs for 25 min, which demonstrated its potential use in energy-storage applications.

7.13. Walnut shells

The shells of walnuts, a popular nut, were used by Wang et al. to produce activated porous carbon (WSs), which, in turn, was used as the negative electrode material in an ASC.[151] The waste walnut shells were pulverized and annealed at 800 °C under an argon atmosphere and subsequently activated with HNO_3 to produce WSs. The graphitic phase was identified by means of XRD analysis and N_2 adsorption–desorption measurements, which confirmed the presence of mesopores with an average size of 2.8 nm and a large surface area of 366 $m^2 g^{-1}$. This highly porous material displayed a high specific capacitance of 137 $F g^{-1}$ at 1 $A g^{-1}$ and retained 96% of its initial capacitance after 5000 cycles. In the search for a suitable positive electrode material, the authors employed $NiCo_2O_4$ as the positive electrode to construct the ASC, which is a cost-effective, environmentally friendly, and high-performance electrode material that can replace expensive RuO_2 in ASC applications. Therefore, $NiCo_2O_4$ on Ni foam was synthesized through a urea-assisted hydrothermal method, which displayed a nanoneedle-like morphology with diameters in the range of 2–50 nm and an average size of 26 nm, as determined by means of TEM analysis. The specific capacitance of $NiCo_2O_4$ decreased from 461 to 210 $F g^{-1}$ as the current density was increased from 0.5 to 5 $A g^{-1}$. However, $NiCo_2O_4$/WSs in 2 M KOH delivered only 52.3 $F g^{-1}$ at 0.5 $A g^{-1}$, although a noticeable energy density of 21 $Wh kg^{-1}$ was observed at a power density of 0.42 $kW kg^{-1}$ and ensured 99.3% capacitance retention after 5000 cycles at 4 $A g^{-1}$.

7.14. Almond shells

Activated microporous carbon (AMC) derived from almond shells, for use in high energy density ASCs, was studied by Wu et al.[122] The synthesis of AMC from natural almond shell waste was successfully carried out through the activation of carbonized almond shells with HNO_3 or KOH. In the first method, the carbonized material, which was heated at 800 °C for 2 h, was further activated with KOH in a 1:4 ratio at 800 °C for 2 h after impregnation at 80 °C for 6 h. In the second method, 16 M HNO_3 was used to impregnate the carbonized material at 60 °C for 24 h. Additionally, the ternary oxide Zn–Ni–Co (ZNCO) was synthesized through a facile hydrothermal reaction followed by calcination. However, the carbon material without any activation displayed porous structures and showed an interplanar spacing of 0.34 nm, which was attributed to the graphitic texture. Similarly, the HNO_3-AC displayed the same characteristics, and micropores were observed for the KOH-AC. Among these, the KOH-AC material displayed a large BET surface area of 1363.1 $m^2 g^{-1}$ with the largest pore volume of 0.140 $cm^3 g^{-1}$. The authors reported that the specific capacitances observed for the KOH-AC and HNO_3-AC materials were 272.3 and 286.1 $F g^{-1}$, respectively, at 1 $A g^{-1}$, which were higher than that of the untreated electrode material. Furthermore, it is understood that KOH activation creates more micropores, and activation with HNO_3 introduces heteroatoms and functional groups onto the carbon surface, which increases the capacitance of the chemically activated materials. The ASC devices assembled with ZNCO as the positive electrode showed a high specific capacitance of 170 and 172 $F g^{-1}$ in 6 M KOH, if paired with the KOH-AC and HNO_3-AC electrodes, respectively. The ZnCO/HNO_3-AC ASC exhibited a high energy density of 53.6 $Wh kg^{-1}$ at a power density of 1.12 $kW kg^{-1}$, with excellent cyclic stability of 83.4% capacitance retention after 5000 cycles; this only very slightly decreased for the ZnCO/KOH-AC ASC.

7.15. Corncob

Liu et al. prepared hierarchical nickel cobalt oxide nanoarrays (NCO-NA), consisting of nanosheets (NCO-NS) or nanowires (NCO-NW) on Ni foam and hierarchical porous carbon (Bio-HPC) from corncob-based biowaste for use in ASCs (Figure 14).[152] Bio-HPC, with an interconnected microstructure, was prepared upon pretreatment with KOH in a 1:4 ratio followed by carbonization at 550 °C under an argon atmosphere for 2 h, which exhibited a BET surface area of 745 $m^2 g^{-1}$. In addition, $NiCo_2O_4$-NS was synthesized by depositing the respective metal ions with urea on Ni foam under hydrothermal conditions at 110 °C for 8 h, which exhibited a large surface area of 117.99 $m^2 g^{-1}$. The same procedure was used to synthesize NCO-NW by extending the reaction time to 10 h; this had a surface area of 95.30 $m^2 g^{-1}$, as well as the existing porous nature, as observed by means of TEM analysis. Unexpectedly, the NCO-NW exhibited a high specific capacitance of 2333 $F g^{-1}$, compared with that of NCO-NS, which achieved only 2300 $F g^{-1}$ at 2 $mA cm^{-2}$. However, NCO-NS achieved a higher rate capability than that of NCO-NW. By employing these two materials, the authors fabricated two cost-effective ASC devices, NCO-NS/Bio-HPC and NCO-NW/Bio-HPC, which used 30 wt% KOH solution as the electrolyte and delivered specific capacitances of about 142 and 163 $F g^{-1}$, respectively, over the working voltage window of 1.55 V. Furthermore, the ASC constructed from NCO-NW/Bio-HPC exhibited a high energy density of 54.44 $Wh kg^{-1}$ at 124.99 $W kg^{-1}$, whereas NCO-NS/Bio-HPC ASC showed 47.44 $Wh kg^{-1}$ at 0.14 $kW kg^{-1}$. However, the NCO-NS/Bio-HPC ASC outshone the NCO-NW/Bio-HPC ASC in terms of its cycling stability due to its unique 2D texture; it lost only about 8.88% of its initial capacitance after 2000 cycles, whereas NCO-NW/Bio-HPC ASC was able to retain 77.48% capacitance in the same test. Practically, both ASCs are able to efficiently power a blue LED indicator after being connected in series (Figure 14 f).

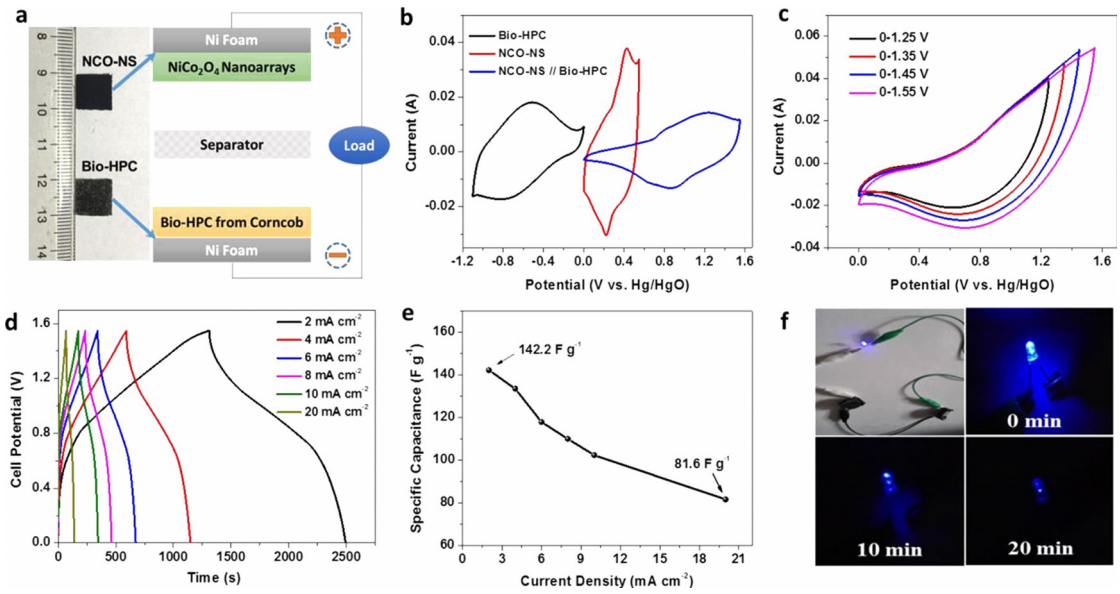

Figure 14. a) A schematic illustration of the NCO-NS/Bio-HPC ASC. b) CV curves obtained for NCO-NS and Bio-HPC in a single-electrode configuration versus a Hg/HgO electrode and the NCO-NS/Bio-HPC ASC at 5 mV s^{-1}. c) CV traces of the NCO-NS/Bio-HPC ASC over various potential windows at 40 mV s^{-1}. d) GCD curves obtained for NCO-NS/Bio-HPC. e) Specific capacitance (C_s) values of NCO-NS/Bio-HPC at different current densities. f) A photograph showing that two ASCs in series can power a blue LED indicator and the blue LED at different stages (reproduced with permission from Ref. [152]; copyright American Chemical Society, 2017).

7.16. *Pongamia pinnata*/Indian beech

P. pinnata or Karanja is one of the most widely distributed trees in India. It has a diverse range of applications, for example, its oil is used in the production of biodiesel. The application of *Pongamia* seed oil extract cake for the preparation of green carbon, which can be used as electrode material in SCs, was reported, for the first time, by Chaitra et al.[153] The seed oil extract cake is dried at 110 °C for 24 h and then carbonized at 450 °C under an N_2 atmosphere for 1 h. After KOH activation (1:2 and 1:4), the material is calcined under an N_2 atmosphere at 750 °C for 1 h. Drying and neutralization of the resultant material led to the formation of green AC, labeled as KC2 and KC4, respectively. A mixture of nickel and cobalt with different chemical compositions and structural forms proved to be good electrode materials, with advantages such as ease of availability, low cost, eco-friendly nature, and high theoretical specific capacitance. Composites of nickel and cobalt prepared with non-faradaic carbon materials, such as MWCNTs, have been found to increase the electrochemical properties. Due to their tubular mesoporous network, high electrical conductivity, mechanical stability, and large surface area available for redox reactions, MWCNTs are commonly used as conducting materials for metal oxides. The estimated specific capacitance values for green AC and its composite electrode material at 10 mV s^{-1} were 233 and 1837 F g^{-1}, respectively. The authors assembled an ASC by using green AC as the negative electrode and a nanocomposite of Ni–Co@MWCNTs as the positive electrode in 1 M KOH electrolyte. The device offered a specific capacitance of 177 F g^{-1} at 10 mV s^{-1} with energy and power densities of 44 Wh kg^{-1} and 18 kW kg^{-1}, respectively. The device also showed 92% capacitance retention after 3000 cycles and could effectively power a calculator for more than 1 h.

7.17. *Cladophora glomerata*

Pourhosseini et al. developed a novel interconnected 3D porous network containing iron nanoparticles from harmful marine biomass, *Cladophora* glomerate (CG), which was utilized as an electrode material in ASCs.[154] CG was stirred in a solution of $FeCl_3$ and the dried material was then pyrolyzed at 700 °C for 4 h under an argon atmosphere to give magnetic biochar (MBC). Furthermore, functional biochar (FBC) was prepared by mixing dried microalgae with 6 M KOH or refluxing H_2SO_4 and HNO_3 at 80 °C for 6 h. The resulting suspensions were pyrolyzed at 700 °C for 2 h to create a 3D pore network structure. Finally, the iron composite biochar (FCBC) was prepared through the reduction of FBC with $FeSO_4$ under hydrothermal conditions at 120 °C for 15 h. The three biochars, MBC, FBC, and FCBC, exhibited BET surface areas of 475, 670, and 957 m^2 g^{-1}, respectively. At a current density of 1 A g^{-1}, the maximum values of specific capacitance obtained for the MBC, FBC, and FCBC electrodes were 299, 332, and 427 F g^{-1}, respectively. Among these biochars, the higher graphitic character of FCBC was observed through Raman spectroscopy; this was attributed to the reduction reaction with iron particles conducted under hydrothermal conditions. The authors reported that FCBC showed good capacitive behavior, with a cycling performance of 102.1% after 10000 cycles. The authors also assembled an ASC by using FBC as the negative electrode and FCBC as the positive electrode in 3 M KCl electrolyte, which exhibited a high specific capacitance of 369 F g^{-1} at 1 A g^{-1}. Remarkably, the device delivered an energy density of 41.5 Wh kg^{-1} at a power density of 0.90 kW kg^{-1}, with a stable cycling performance of 10000 cycles at 8 A g^{-1} with 93.1% capacitance retention over a wide potential window.

7.18. Jackfruit peel

Jackfruit (JF; *Artocarpus heterophyllus*) is a popular fruit used across the world, which is not in or out of season. JF peel waste has no economic value and, due to the large quantity of waste produced, it can create a serious disposal problem. It has a high carbon content with heterogeneous porous microstructures and various functionalities. Sennu et al. fabricated an ASC by using JF peel-derived high surface area porous carbon as the negative electrode and a pseudocapacitive 3D microstructured $NiCo_2O_4$@Co_3O_4 composite as the positive electrode.[155] Waste wet skin of JF was washed, cut into small pieces, and charred at 150 °C for 1 h. Activation of the resulting black char was carried out with KOH (weight ratio = 1:2) at 120 °C for 3 h. JF-derived AC was produced by further heating the material to 800–900 °C under a nitrogen atmosphere at a heating rate of 5 °C. The XRD pattern showed the absence of sharp and strong reflections for JF-derived AC, which indicated the presence of a randomly oriented amorphous phase that was attributed to the high activation temperature. The porous nature of the electrode materials was studied by means of N_2 adsorption–desorption isotherms. The SSA of JF-derived AC was found to be 2235 $m^2 g^{-1}$ and that of $NiCo_2O_4$@Co_3O_4 was 73.43 $m^2 g^{-1}$. The fabricated ASC, in the presence of 2 M KOH electrolyte, exhibited a high energy density of 42.5 Wh kg^{-1} at a power density of 0.08 kW kg^{-1}. This device also delivered a high specific capacitance of 119 F g^{-1} and about 97% capacitance retention after 7000 cycles.

7.19. Popcorn pieces

Yu et al. successfully enhanced the electrochemical activity of popcorn-derived activated carbon (PC), which was obtained from maize grain, by using a $NiCo_2S_4$ nanoparticle coating for application in ASCs.[156] PC was produced through carbonization of popcorn pieces under a nitrogen atmosphere followed by mixing the resultant material with a solution of KOH and pyrolysis at 800 °C. XRD analysis confirmed the amorphous nature of PC by the presence of two peaks at 24.6 and 43.5°, which were ascribed to the (002) and (100) planes, respectively. In addition, the authors developed a $NiCo_2S_4$@PC composite upon anchoring dispersed $NiCo_2S_4$ nanoparticles onto the surface of PC under hydrothermal conditions by employing sodium sulfide as a sulfur source. After confirmation of the growth of $NiCo_2S_4$ on PC by XRD and Raman spectroscopy, ball-like nanoparticles on the surface of PC were observed in the composite during SEM analysis, which indicated the growth of $NiCo_2S_4$ during the course of the hydrothermal reaction. In addition, the large surface area of PC (1218.4 $m^2 g^{-1}$) can act as a substrate to hold the $NiCo_2S_4$ active materials. However, a low surface area of 525 $m^2 g^{-1}$ was obtained for the resultant composite because the pores in the PC material were blocked. However, the composite showed a high specific capacitance of 605 F g^{-1} at a current density of 0.5 A g^{-1} in 6 M KOH electrolyte, which proved that the surface area offered sufficient contact between the electrolyte and active materials for transport. Furthermore, the device showed 92.7% capacitance retention after 5000 charge–discharge cycles at a high current density of 10 A g^{-1}. Meanwhile, the ASC also revealed a high energy density of 23.3 Wh kg^{-1} at a power density of 0.34 kW kg^{-1}, which demonstrated its potential application in energy-storage devices.

7.20. Corn bract

An aqueous electrolyte based ASC prepared with a 1D nanostructure formed from nitrogen-doped porous carbon material (CBC) based on agricultural corn bract waste as the positive electrode and pseudocapacitive $K_{0.3}WO_3$ as the negative electrode with 1 M H_2SO_4 electrolyte was fabricated by Ma et al.[59] CBC was prepared through the carbonization of corn bract under a nitrogen atmosphere followed by $ZnCl_2$ activation. Dried corn bract and $ZnCl_2$ were mixed in a 1:1 ratio and pyrolyzed at 800 °C for 2 h, which improved the pore volume and surface area up to 0.5 $cm^3 g^{-1}$ and 820.6 $m^2 g^{-1}$, respectively. The resultant material exhibited a turbostratic carbon structure in XRD analysis, with two broad characteristic peaks at 25.5 and 43.7°, which corresponded to the (002) and (100) reflections, respectively. Moreover, the coexistence of micro- (< 2 nm) and mesopores (2–5 nm) with coral-like frameworks facilitated effective ion transport between the electrode/electrolyte interfaces to enhance the electrochemical performance. In addition, a two-step hydrothermal reaction was used in the synthesis of the $K_{0.3}WO_3$ nanorods. In the first step, WO_3 was synthesized through a NaCl-assisted hydrothermal reaction at 180 °C for 24 h. In the next step, dispersed WO_3 was treated with KSCN and the homogeneous solution was heated at 180 °C for 24 h. The as-obtained material had a surface area of 18.5 $m^2 g^{-1}$ and a structure composed of 1D thin nanorods. A high specific capacitance of 224 F g^{-1} was obtained for $K_{0.3}WO_3$ at 0.8 A g^{-1}, despite CBC having a specific capacitance of 245 F g^{-1} at a current density of 0.5 A g^{-1} and 92% capacitance retention after 5000 consecutive cycles. The redox character of $K_{0.3}WO_3$ and fast ion-transport properties of CBC were the two factors that led to the fabrication of the ASC with BDC as a positive electrode, for the first time. The assembled ASC in 1 M H_2SO_4 delivered a notable capacitance of 296 F g^{-1} at 0.5 A g^{-1} with high energy and power densities of 26.3 Wh kg^{-1} and 0.4 kW kg^{-1}, respectively, over a wide voltage window of 0–1.6 V.

7.21. Wheat straw

Recently, Fang et al. synthesized biomass-derived porous carbon (BPC) by using a common agricultural waste, wheat straw, as a precursor, which was decorated with ultrathin Fe_2O_3 film to form a Fe_2O_3@BPC nanocomposite.[157] The synthesis of BPC was carried out through KOH activation of wheat straw at 800 °C for 2 h under an argon atmosphere. The authors reported that the BPC produced consisted of a 3D interconnected macroporous structure with short-range graphitic domains and a large number of micropores. The preparation of the hierarchically nanostructured nanocomposite was accomplished by casting $Fe(NO_3)_3$ onto the surface of BPC, followed by a postan-

nealing treatment. The composite exhibited the characteristics of both redox reactions and EDLC, but the charge-storage mechanism was dominated by redox reactions. The authors reported that the SSA of both BPC and Fe_2O_3@BPC were 2179.5 and 775.8 $m^2 g^{-1}$, respectively. The authors explained that the large surface area of BPC made it an ideal matrix for Fe_2O_3. Furthermore, the composite also showed a large specific capacitance of 989 $F g^{-1}$ at a current density of 1 $A g^{-1}$ and retained 82.6% of its initial capacitance, even after 3000 cycles. The ASC assembled from Fe_2O_3@BPC as the negative electrode and CNT@Co–Ni LDH as the positive electrode in 3 M KOH electrolyte delivered a high open-circuit voltage of 1.6–1.65 V. The ASC also exhibited a high specific energy of 96.7 $Wh kg^{-1}$ and a specific power of 20.65 $kW kg^{-1}$.

7.22. Ginkgo leaf

Fu and co-workers prepared ginkgo leaf derived nitrogen-doped carbon, which was used as an electrode active material for ASC applications.[158] Ginkgo biloba leaf was carbonized at 900 °C for 1 h; this was denoted as gingko biloba leaf derived carbon (GLC). To prepare a jellylike slurry, GLC powder was activated with 45 wt% aqueous KOH mixed in a 1:4 ratio, heated at 100 °C, followed by calcination at 900 °C for 1 h. The KOH-activated GLC (KGLC) was used to produce porous N-doped KOH-activated GLC (NKGLC) through dispersion in a solution of NH_3 under hydrothermal conditions at 180 °C for 12 h. TEM analysis revealed the disordered structure of NKGLC with rough edges; the coexistence of micro- and macropores favors ion diffusion because it has a large BET surface area of 905.9 $m^2 g^{-1}$ and pore volume of 0.40 $cm^3 g^{-1}$. XPS analysis indicated its high nitrogen content (pyridinic and pyrrolic N species), which, if accompanied by the hierarchical porous structure of NKGLC, led to an enhanced capacitance of 345 $F g^{-1}$ at 0.2 $A g^{-1}$, compared with those of GLC ($\approx$75 $F g^{-1}$) and KGLC ($\approx$300 $F g^{-1}$). The authors also fabricated an ASC by using NKGLC as the negative electrode and a $Ni(OH)_2$–MnO_2–rGO composite as the positive electrode in 1 M KOH, which delivered a maximum energy density of 42.2 $Wh kg^{-1}$ at 700 $W kg^{-1}$, with a satisfactory electrochemical cycling stability over 3000 cycles, retaining 70% of its initial capacitance. These results demonstrate the significance of nitrogen doping, which may improve the electrochemical importance and further indicates that biomass-derived KGLC is a good candidate for the construction of low-cost, high-performance ASCs.

7.23. *Salvia splendens*

Huang et al. reported that the high theoretical capacitance of MnO_2 as a positive electrode material could only be effectively utilized in nanostructured forms.[159] The effective capacitance value can be increased by compositing it with highly conductive carbon-based porous materials. Previous studies have shown that graphene-like porous carbon nanosheets (GPCNs) have great potential in SC applications.[160] In a recent study, Liu et al. demonstrated a novel ASC composed of MnO_2 nanostructures and biomass *Salvia splendens* (SS)-based GPCNs, which was prepared through the pyrolysis of NaCl crystal sealed SS petals at 800 °C for 2 h under a nitrogen atmosphere, followed by washing and drying.[161] The authors reported the direct deposition of MnO_2 nanostructures onto the surface of biomass-derived GPCNs (GPCN-SS) through a hydrothermal reaction.[135] The MnO_2@GPCN-SS composite exhibited a suitable mesopore distribution of 2–5 nm and SSA of 483 $m^2 g^{-1}$. Due to the synergistic effects of its components, the composite can deliver a specific capacitance of 438 $F g^{-1}$ at a current density of 0.5 $A g^{-1}$, as well as a high rate capability in a Na_2SO_4 electrolyte. The authors also fabricated an ASC by using the MnO_2@GPCN-SS composite as the positive electrode and GPCN-SS as the negative electrode in a neutral electrolyte, which could deliver an energy density of 50.2 $Wh kg^{-1}$ at 0.52 $kW kg^{-1}$ with 77.8% capacity retention. Furthermore, the authors concluded that, due to the abundance and sustainability of the biomass-derived GPCNs, along with the low cost of MnO_2, the MnO_2@GPCN-SS composite was a promising electrode material for SC applications (Figure 15).

8. Summary and Outlook

The above-discussed reports clearly demonstrate that chemical activation with activating agents (such as KOH, NaOH, and $ZnCl_2$) is an extremely promising strategy for the preparation highly micro- and mesoporous BDC materials for use in high-capacitance electrodes. Nevertheless, KOH activation is unable to offer graphitic carbon materials, which result in high electrical conductivity and good surface wettability toward the electrolyte. However, some biomass precursors deliver high capacitance, but their low carbon yield limits their large-scale production. Therefore, to attain a high carbon yield, the carbonization efficiency needs to be improved by initially extracting the major carbon donors for purification, which can then be concentrated prior to thermal treatment. Moreover, the addition of metallic catalysts will enrich the formation of graphitic structures, and their organic compounds can be used as an additional carbon source in the carbonization process. In addition, the combination of KOH activation and carbonization in a one-pot process is favorable for the formation of BDC materials with large surface areas and the advantages of controllable pore structures, notable electrical conductivity, and high wettability toward the electrolyte. Correspondingly, some biomass sources inherently grasp heteroatoms and metal ions that further facilitate an increase in the overall capacitance of an ASC through their advantageous properties; this has led researchers to focus on BDC electrodes. Industry also wants simple techniques, which can produce these materials by using short routes with the benefit of low cost. Consequently, a facile procedure that combines KOH activation and thermal treatment may overcome the intrinsic steps and high temperatures used in a physical activation process.

In addition, recently studied ASC devices constructed from BDC-based electrodes have been discussed, and it is clear that these materials can be used to construct high energy and power density ASCs, compared with conventional EDLCs. The development of ASCs with a BDC capacitive electrode and a

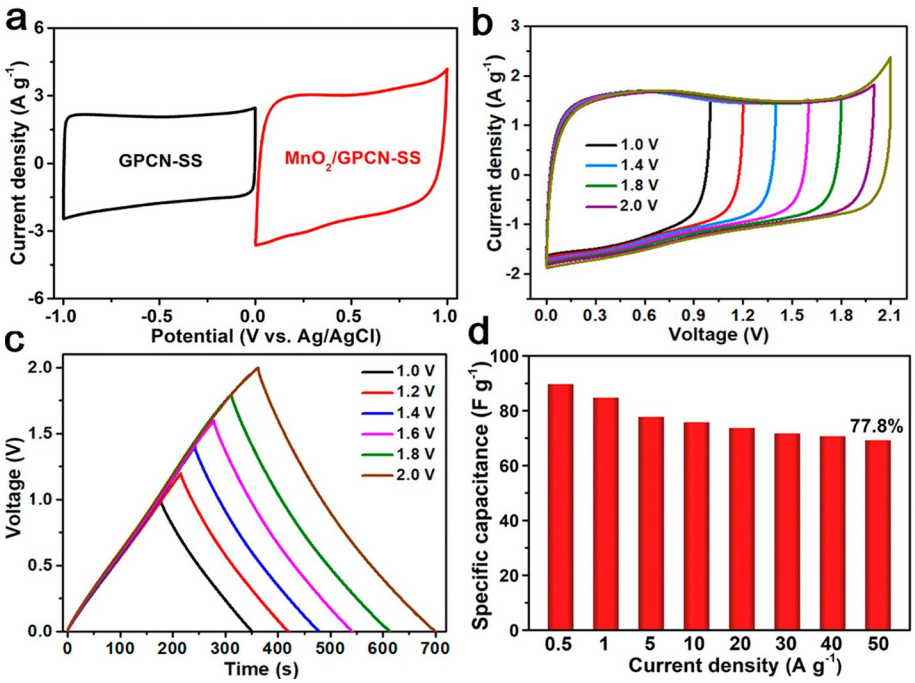

Figure 15. a) CV curves obtained for GPCN-SS and MnO_2@GPCN-SS at 10 mV s^{-1} in a three-electrode setup with 1 M Na_2SO_4 electrolyte. b) CV profiles obtained at 10 mV s^{-1}. c) GCD profiles obtained at 0.5 A g^{-1} with different operating voltages. d) The correlation between the specific capacitance and current density of the MnO_2@GPCN-SS/GPCN-SS ASC in 1 M Na_2SO_4 (reproduced with permission from Ref. [135]; copyright American Chemical Society, 2019).

low-cost pseudocapacitive electrode is a promising approach, which can widen the operating voltage window, and hence, lead to the construction of devices with improved energy density and specific capacitance. From the viewpoint of the reported studies, the utilization of BDC electrodes as the negative electrode and a composite of BDC and any low-cost pseudocapacitive material (such as MnO_2) can form cost-effective ASCs (Figure 16). From the results in Figure 16, we can see high energy with high power capability is obtained for the GPCN-SS/MnO_2@GPCN-SS-based ASC, mainly because of the utilization of the pseudocapacitive MnO_2 electrode. On the other hand, the battery-type material Co–Ni LDH dominates in energy due to perfect faradaic reactions at lower rates. However, as expected, under harsh conditions, the Co–Ni LDH based ASC was rendered with an inferior power capability to that of pseudocapacitive-type MnO_2-based ASCs; this was mainly due to diffusion-limited kinetics. Generally, these devices have advantages such as low-cost production and excellent performance, which make them a good choice for the next generation of renewable energy-storage systems to meet future energy demands.

Generally, carbon materials can deliver high-level performance; however, they face issues such as a limited range of specific capacitance. On the other hand, metal oxides that display pseudocapacitive behavior generally exhibit poor stability, low conductivity, and low durability. The best way to achieve the maximum performance of an electrode material is to construct a composite that merges both EDLC and pseudocapacitive behavior to accomplish a high specific capacitance, compared with that of the individual characteristics of the materials. For instance, the combination of a biomass-derived composite electrode (BDCE), which comprises a BDC with a metal oxide, a conducting polymer, or a combination of both, has the ability to produce outstanding capacitance rela-

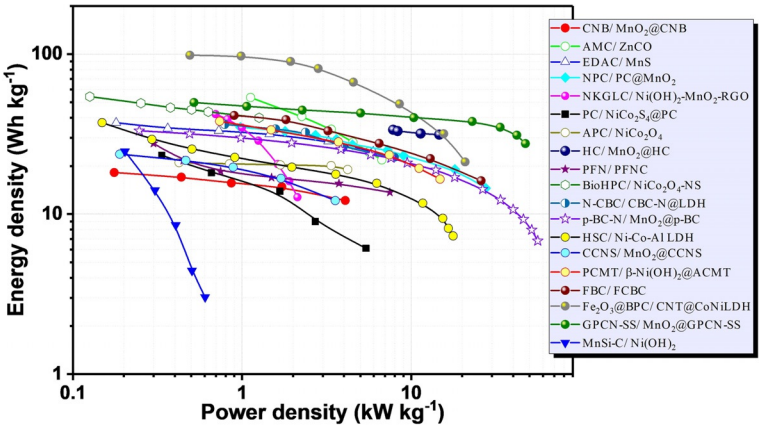

Figure 16. A comparison of the Ragone plots obtained for ASCs constructed from BDC materials reported herein. CNB/MnO_2@CNB (BDC = tofu),[128] AMC/ZnCO (BDC = almond shells),[122] EDAC/MnS (BDC = eggplant),[145] NPC/PC@MnO_2 (BDC = loofah sponge),[130] NKGLC/$Ni(OH)_2$–MnO_2–rGO (BDC = ginkgo leaf),[158] PC/$NiCo_2S_4$@PC (BDC = popcorn pieces),[156] APC/$NiCo_2O_4$ (BDC = walnut shells),[151] HC/MnO_2@HC (BDC = hemp stems),[126] PFN/PFNC (BDC = pomelo fruit),[150] BioHPC/$NiCo_2O_4$-NS (BDC = corncob),[152] N-CBC/CBC-N@LDH (BDC = bacterial cellulose pellicles),[133] p-BC-N/MnO_2@p-BC (BDC = bacterial cellulose pellicles),[87] HSC/Ni-Co-Al LDH (BDC = bacterial cellulose pellicles),[134] CCNS/MnO_2@CCNS (BDC = willow catkin)[57] PCMT/β-$Ni(OH)_2$@ACMT (BDC = willow catkin),[89] FBC/FCBC (BDC = CG),[154] Fe_2O_3@BPC/CNT@CoNiLDH (BDC = wheat straw),[157] GPCN-SS/MnO_2@GPCN-SS (BDC = SS),[135] and MnSi-C/$Ni(OH)_2$ (BDC = bamboo leaves).[147]

tive to the capacitance of the metal oxides or conducting polymers themselves. This type of electrode can involve both physical and chemical charge-storage mechanisms and may overcome the low electrochemical performance observed in energy-storage devices. Recent reports have employed BDCEs as positive electrodes and BDCs as negative electrodes to develop low-cost, high-performance ASCs. In this case, MnO_2- or Fe_2O_3-based BDCEs are great choices as the positive electrode for high-performance ASCs due to their low toxicity and cost-effectiveness compared with other metal oxides, which may result in enhanced electrochemical performance, in terms of the energy and power density.

In addition, it is a prerequisite to establish a detailed procedure for any new electrode material, so that it can be replicated in another laboratory. Most importantly, the ratio of active material, binder, and conductive agents used in the electrode fabrication procedure should be clearly reported. Moreover, researchers are recommended to include the mass of active material loading per electrode area (i.e., $mg\,cm^{-2}$). Thus, one can assess the electrochemical performance of an active material and the full device, as well as comparing them with other active materials. Similarly, the composition of a new electrolyte and other properties, including the density, ionic conductivity, boiling point, and viscosity at room temperature, should be presented in the reported study. In addition, information on the electrochemical stability of a newly proposed electrolyte will help readers in their experiments. Due to the nonexistence of a standard procedure, it would be better to evaluate the electrochemical potential window of each electrolyte because the operating voltage mostly relies on the electrochemical stability of the electrolyte in the electrodes based on the capacitive materials. However, the potential range over which the faradaic charge-storage process determines the electrochemical potential window of pseudocapacitive materials used to design a two-electrode system. Apart from these parameters, the cycling stability is a significant parameter used to estimate the device configuration for ASCs. The values of the voltage range, current density, and cycling life for an ASC should be specified, in that capacitive material-based devices are advised to report a minimum of 10000 cycles, whereas 5000 cycles are essential for pseudocapacitive materials. A float test is also helpful to gain more information to estimate the cycling stability of devices and should be performed for a minimum of 50–100 h at a constant voltage. Additionally, we are strongly encouraging researchers to provide the capacity values obtained for capacitive materials in $C\,g^{-1}$ (or $mA\,h\,g^{-1}$) instead of $F\,g^{-1}$, except for MnO_2 and RuO_2. When comparing the capacitance or rate capability values of various materials, the readers ought to consider the thickness of the electrodes/devices.

Nevertheless, there are many issues that hinder the development of biomass-derived electrode-based ASCs. One of these issues is the selection of a suitable biomass precursor, which can result in a carbon material with the required qualities. Due to the diversity of biomass precursors, there is a great demand for further research to find the relationship between biomass composition and the electrochemical performance of the as-produced carbon materials. This will help researchers make ASCs from selected biomass precursors. It is also important to formulate some standard protocol for electrode fabrication and the measurement of the capacitance and potential window, which can ensure more accurate results. Most of the reported studies regarding biomass-derived electrode materials with considerable performance have only been developed on a laboratory scale. Also, it should be noted that the requirement for excess electrode material has become a disadvantage in the practical fabrication of ASCs. There is a need for next-level research to scale up and further develop this technology. We also hope that an appropriate understanding of biomass precursor selection will support the fabrication of ASCs, thereby promoting low-cost, biomass-based, high-performance ASCs as future environmentally and economically friendly energy-storage systems.

Currently, cradle-to-grave analysis scrutinizes the potential environmental impact of solution-oriented technologies, which emphasizes need to adapt the resultant products for recycling and their biodegradability. Most of the studies reported reveal that the utilization of biomass as a precursor for ASC electrode materials is a good approach, which may lead to the further development of energy-storage systems. In the future, the increasing use of biofuels and efforts toward the reduction of greenhouse gas emissions are predicted to produce a colossal quantity of valuable biomass compounds as byproducts, which will have prospects as economically feasible biomass-related precursors. Apart from this, biomass opens up an innovative research area, offering flexible fibers or foams as electrodes to fabricate flexible ASC devices because the demand for these materials in portable electronics applications is increasing daily. However, we all expect that low-cost, commercially available, biomass-derived ASCs prepared by using easier techniques will preserve the environment by implementing zero-transport transmissions in the future.

Acknowledgements

V.A. acknowledges financial support from the Science & Engineering Research Board (SERB), a statutory body of the Department of Science & Technology, Govt. of India, through a Ramanujan Fellowship (SB/S2/RJN-088/2016). Y.S.L. acknowledges the Ministry of Science, ICT, and Future Planning of South Korea for providing a National Research Foundation of Korea (NRF) grant (no. 2019R1A4A2001527).

Conflict of interest

The authors declare no conflict of interest.

Keywords: asymmetric supercapacitors · biomass · electrochemistry · energy storage · renewable resources

[1] Z. Yang, J. Zhang, M. C. W. Kintner-Meyer, X. Lu, D. Choi, J. P. Lemmon, J. Liu, *Chem. Rev.* **2011**, *111*, 3577.
[2] New Energy Outlook 2018, https://about.bnef.com/blog/global-electricity-demand-increase-57-2050/.

[3] https://en.wikipedia.org/wiki/Electricity_sector_in_India.
[4] S. Zhang, *Front. Energy Res.* **2013**, *1*, 8.
[5] T. K. Enock, King, C. K. King'ondu, A. Pogrebnoi, Y. A. C. Jande, *Int. J. Electrochem.* **2017**, 14.
[6] https://www.forbes.com/sites/sarwantsingh/2018/04/03/global-electric-vehicle-market-looks-to-fire-on-all-motors-in-2018/.
[7] A. Gulagi, D. Bogdanov, C. Breyer, *Energy Procedia* **2017**, *135*, 37.
[8] D. Larcher, J. M. Tarascon, *Nat. Chem.* **2015**, *7*, 19.
[9] N. Dominguez, B. Torres, L. A. Barrera, J. E. Rincon, Y. R. Lin, R. R. Chianelli, M. A. Ahsan, J. C. Noveron, *ACS Omega* **2018**, *3*, 10243.
[10] H. Chen, T. N. Cong, W. Yang, C. Tan, Y. Li, Y. Ding, *Prog. Nat. Sci.* **2009**, *19*, 291.
[11] A. K. Shukla, S. Sampath, K. Vijayamohanan, *Curr. Sci.* **2000**, *79*, 1656.
[12] P. Svasta, R. Negroiu, A. Vasile, Supercapacitors—an Alternative Electrical Energy Storage Device, *5th International Symposium on Electrical and Electronics Engineering (ISEEE)*, Oct 20 – 22, **2017**.
[13] A. González, E. Goikolea, J. A. Barrena, R. Mysyk, *Renewable Sustainable Energy Rev.* **2016**, *58*, 1189.
[14] Digital Journal Press Release, Global Supercapacitors Market to Witness Soaring Growth During 2018 – 2028; http://www.digitaljournal.com/pr/3830500.
[15] N. Choudhary, C. Li, J. Moore, N. Nagaiah, L. Zhai, Y. Jung, J. Thomas, *Adv. Mater.* **2017**, *29*, 1605336.
[16] S. Herou, P. Schlee, A. B. Jorge, M. Titirici, *Curr. Opin. Green Sustainable Chem.* **2018**, *9*, 18.
[17] B. Zhu, B. Liu, C. Qu, H. Zhang, W. Guo, Z. Liang, F. Chen, R. Zou, *J. Mater. Chem. A* **2018**, *6*, 1523.
[18] V. Subramanian, C. Luo, A. M. Stephan, K. S. Nahm, S. Thomas, B. Wei, *J. Phys. Chem. C* **2007**, *111*, 7527.
[19] B. Xu, H. Duan, M. Chu, G. Cao, Y. Yang, *J. Mater. Chem. A* **2013**, *1*, 4565.
[20] Z. Fan, D. Qi, Y. Xiao, J. Yan, T. Wei, *Mater. Lett.* **2013**, *101*, 29.
[21] J. Liu, Y. Deng, X. Li, L. Wang, *ACS Sustainable Chem. Eng.* **2016**, *4*, 177.
[22] K. Byungwoo, C. Haegeun, K. Woong, *Nanotechnology* **2012**, *23*, 155401.
[23] M. Jayalakshmi, K. Balasubramanian, *Int. J. Electrochem. Sci.* **2008**, *3*, 1196.
[24] E. Gongadze, S. Petersen, U. Beck, U. van Rienen, Classical Models of the Interface between an Electrode and an Electrolyte, *Cosmol Conference*, Milan, **2009**.
[25] Y. Shao, M. F. El-Kady, J. Sun, Y. Li, Q. Zhang, M. Zhu, H. Wang, B. Dunn, R. B. Kaner, *Chem. Rev.* **2018**, *118*, 9233.
[26] W. Zuo, R. Li, C. Zhou, Y. Li, J. Xia, J. Liu, *Adv. Sci.* **2017**, *4*, 1600539.
[27] M. Yassine, D. Fabris, *Energies* **2017**, *10*, 1340.
[28] U. Sani, *AKGEC Int. J. Technol.* **2015**, *6*, 36.
[29] P. Simon, Y. Gogotsi, *Nat. Mater.* **2008**, *7*, 845.
[30] V. K. Mariappan, K. Krishnamoorthy, P. Pazhamalai, S. Sahoo, S. S. Nardekar, S.-J. Kim, *Nano Energy* **2019**, *57*, 307.
[31] Y. Wang, Y. Song, Y. Xia, *Chem. Soc. Rev.* **2016**, *45*, 5925.
[32] K. Jost, G. Dion, Y. Gogotsi, *J. Mater. Chem. A* **2014**, *2*, 10776.
[33] L. L. Zhang, X. S. Zhao, *Chem. Soc. Rev.* **2009**, *38*, 2520.
[34] Y. Zhai, Y. Dou, D. Zhao, P. F. Fulvio, R. T. Mayes, S. Dai, *Adv. Mater.* **2011**, *23*, 4828.
[35] M. Gidwani, A. Bhagwani, N. Rohra, *Int. J. Eng. Invent.* **2014**, *4*, 22.
[36] M. R. Lukatskaya, B. Dunn, Y. Gogotsi, *Nat. Commun.* **2016**, *7*, 12647.
[37] Z. S. Iro, C. Subramani, S. S. Dash, *Int. J. Electrochem. Sci.* **2016**, *11*, 10628.
[38] X. Shi, S. Zheng, Z.-S. Wu, X. Bao, *J. Energy Chem.* **2018**, *27*, 25.
[39] T. Brousse, D. Bélanger, J. W. Long, *J. Electrochem. Soc.* **2015**, *162*, A5185.
[40] B. E. Conway, *Electrochemical Supercapacitors: Scientific Fundamentals and Technological Applications*, Springer, New York, **2013**.
[41] Y. Gogotsi, R. M. Penner, *ACS Nano* **2018**, *12*, 2081.
[42] V. Augustyn, P. Simon, B. Dunn, *Energy Environ. Sci.* **2014**, *7*, 1597.
[43] T. C. Liu, W. G. Pell, B. E. Conway, *Electrochim. Acta* **1999**, *44*, 2829.
[44] B. E. Conway, *J. Electrochem. Soc.* **1991**, *138*, 1539.
[45] T. Brousse, D. Bélanger, D. Guay in *Supercapacitors: Materials, Systems, and Applications* (Eds.: F. Béguin, E. FrackowiakB. E. Conway), Wiley-VCH, Weinheim, **2013**, pp 257 – 288.
[46] V. Augustyn, J. Come, M. A. Lowe, J. W. Kim, P.-L. Taberna, S. H. Tolbert, H. D. Abruña, P. Simon, B. Dunn, *Nat. Mater.* **2013**, *12*, 518.
[47] S. Roldán, D. Barreda, M. Granda, R. Menéndez, R. Santamaría, C. Blanco, *Phys. Chem. Chem. Phys.* **2015**, *17*, 1084.
[48] M. Yu, D. Lin, H. Feng, Y. Zeng, Y. Tong, X. Lu, *Angew. Chem. Int. Ed.* **2017**, *56*, 5454; *Angew. Chem.* **2017**, *129*, 5546.
[49] H. Jin, X. Feng, J. Li, M. Li, Y. Xia, Y. Yuan, C. Yang, B. Dai, Z. Lin, J. Wang, J. Lu, S. Wang, *Angew. Chem. Int. Ed.* **2019**, *58*, 2397; *Angew. Chem.* **2019**, *131*, 2419.
[50] M. Yu, Y. Lu, H. Zheng, X. Lu, *Chem. Eur. J.* **2018**, *24*, 3639.
[51] M. G. Bakker, R. M. Frazier, S. Burkett, J. E. Bara, N. Chopra, S. Spear, S. Pan, C. Xu, *Nanomater. Energy* **2012**, *1*, 136.
[52] H. Lu, X. S. Zhao, *Sustainable Energy Fuels* **2017**, *1*, 1265.
[53] W. Gu, G. Yushin, *Wiley Interdisciplinary Rev. Energy Environ.* **2014**, *3*, 424.
[54] T. K. Enock, King, C. K. King'ondu, A. Pogrebnoi, Y. A. C. Jande, *Int. J. Electrochem.* **2017**, 6453420.
[55] W. Ma, H. Nan, Z. Gu, B. Geng, X. Zhang, *J. Mater. Chem. A* **2015**, *3*, 5442.
[56] P.-C. Chen, G. Shen, Y. Shi, H. Chen, C. Zhou, *ACS Nano* **2010**, *4*, 4403.
[57] Y. Li, N. Yu, P. Yan, Y. Li, X. Zhou, S. Chen, G. Wang, T. Wei, Z. Fan, *J. Power Sources* **2015**, *300*, 309.
[58] Q.-Z. Zhang, D. Zhang, Z.-C. Miao, X.-L. Zhang, S.-L. Chou, *Small* **2018**, *14*, 1702883.
[59] G. Ma, Z. Zhang, K. Sun, E. Feng, H. Peng, X. Zhou, Z. Lei, *J. Power Sources* **2016**, *330*, 219.
[60] M. Yang, Z. Zhou, *Adv. Sci.* **2017**, *4*, 1600408.
[61] Y. Gogotsi, P. Simon, *Science* **2011**, *334*, 917.
[62] J. Chmiola, C. Largeot, P.-L. Taberna, P. Simon, Y. Gogotsi, *Science* **2010**, *328*, 480.
[63] *Nanomaterials Handbook* (Ed.: Y. Gogotsi), CRC Press, Boca Raton, **2006**.
[64] J. Chmiola, G. Yushin, Y. Gogotsi, C. Portet, P. Simon, P. L. Taberna, *Science* **2006**, *313*, 1760.
[65] J. Barkauskas, M. Dervinyte, *J. Serb. Chem. Soc.* **2004**, *69*, 363.
[66] F. Béguin, V. Presser, A. Balducci, E. Frackowiak, *Adv. Mater.* **2014**, *26*, 2219.
[67] E. Frackowiak, *Phys. Chem. Chem. Phys.* **2007**, *9*, 1774.
[68] S.-J. Park, Y.-S. Jang, J.-W. Shim, S.-K. Ryu, *J. Colloid Interface Sci.* **2003**, *260*, 259.
[69] R. Xie, Y. Jin, Y. Chen, W. Jiang, *Water Sci. Technol.* **2017**, *76*, 3022.
[70] G. Lota, B. Grzyb, H. Machnikowska, J. Machnikowski, E. Frackowiak, *Chem. Phys. Lett.* **2005**, *404*, 53.
[71] H. Ba, W. Wang, S. Pronkin, T. Romero, W. Baaziz, L. Nguyen-Dinh, W. Chu, O. Ersen, C. Pham-Huu, *Adv. Sustainable Syst.* **2018**, *2*, 1700123.
[72] R. Arenal, K. March, C. P. Ewels, X. Rocquefelte, M. Kociak, A. Loiseau, O. Stéphan, *Nano Lett.* **2014**, *14*, 5509.
[73] D. Hulicova-Jurcakova, M. Seredych, G. Q. Lu, T. J. Bandosz, *Adv. Funct. Mater.* **2009**, *19*, 438.
[74] C. Ma, X. Shao, D. Cao, *J. Mater. Chem.* **2012**, *22*, 8911.
[75] L. Wei, G. Yushin, *Nano Energy* **2012**, *1*, 552.
[76] H. Oda, A. Yamashita, S. Minoura, M. Okamoto, T. Morimoto, *J. Power Sources* **2006**, *158*, 1510.
[77] R. B. Betrián, *Boletín del Grupo Español del Carbón* **2015**, 9.
[78] H. Jin, J. Li, Y. Yuan, J. Wang, J. Lu, S. Wang, *Adv. Energy Mater.* **2018**, *8*, 1801007.
[79] S. Dutta, A. Bhaumik, K. C. W. Wu, *Energy Environ. Sci.* **2014**, *7*, 3574.
[80] Y. Zhao, M. Liu, X. Deng, L. Miao, P. K. Tripathi, X. Ma, D. Zhu, Z. Xu, Z. Hao, L. Gan, *Electrochim. Acta* **2015**, *153*, 448.
[81] D. Hulicova-Jurcakova, M. Seredych, G. Q. Lu, N. K. A. C. Kodiweera, P. E. Stallworth, S. Greenbaum, T. J. Bandosz, *Carbon* **2009**, *47*, 1576.
[82] T. Lin, I.-W. Chen, F. Liu, C. Yang, H. Bi, F. Xu, F. Huang, *Science* **2015**, *350*, 1508.
[83] J. Zhou, J. Lian, L. Hou, J. Zhang, H. Gou, M. Xia, Y. Zhao, T. A. Strobel, L. Tao, F. Gao, *Nat. Commun.* **2015**, *6*, 8503.
[84] M. Sevilla, R. Mokaya, *Energy Environ. Sci.* **2014**, *7*, 1250.
[85] M. Molina-Sabio, F. Rodriguez-Reinoso, *Colloids Surf. A* **2004**, *241*, 15.
[86] F. Rodríguez-Reinoso, M. Molina-Sabio, M. T. González, *Carbon* **1995**, *33*, 15.
[87] L.-F. Chen, Z.-H. Huang, H.-W. Liang, Q.-F. Guan, S.-H. Yu, *Adv. Mater.* **2013**, *25*, 4746.
[88] J. Wang, S. Kaskel, *J. Mater. Chem.* **2012**, *22*, 23710.

[89] Q. Li, C. Lu, D. Xiao, H. Zhang, C. Chen, L. Xie, Y. Liu, S. Yuan, Q. Kong, K. Zheng, J. Yin, *ChemElectroChem* **2018**, *5*, 1279.
[90] J. Li, Z. H. Zhang, D. Wang, Z. Zhu, Z. Q. Fan, G. P. Tang, X. Q. Deng, *Carbon* **2014**, *69*, 142.
[91] H. Yang, S. Kannappan, A. S. Pandian, J.-H. Jang, Y. S. Lee, W. Lu, *arXiv.org e-Print Arch. Condens. Matter* **2013**, arXiv:1311.1413.
[92] O. Barbieri, M. Hahn, A. Herzog, R. Kötz, *Carbon* **2005**, *43*, 1303.
[93] P. Simon, Y. Gogotsi, *Philos. Trans. R. Soc. London Ser. A* **2010**, *368*, 3457.
[94] A. Lewandowski, P. Jakobczyk, M. Galinski, M. Biegun, *Phys. Chem. Chem. Phys.* **2013**, *15*, 8692.
[95] B. E. Conway, W. G. Pell, T. C. Liu, *J. Power Sources* **1997**, *65*, 53.
[96] T. Liu, W. G. Pell, B. E. Conway, *Electrochim. Acta* **1997**, *42*, 3541.
[97] Z. Huang, A. Zhou, J. Wu, Y. Chen, X. Lan, H. Bai, L. Li, *Adv. Mater.* **2016**, *28*, 1703.
[98] Y. Diab, P. Venet, H. Gualous, G. Rojat, *IEEE Trans. Power Electron.* **2009**, *24*, 510.
[99] Z. Gao, Y. Zhang, N. Song, X. Li, *Mater. Res. Lett.* **2017**, *5*, 69.
[100] M. Srivastava, M. Kumar, R. Singh, U. C. Agrawal, M. O. Garg, *J. Sci. Ind. Res. India* **2009**, *68*, 93.
[101] P. Simon, A. Burke, *Electrochem. Soc. Interface* **2008**, *Spring*, 39.
[102] C. Largeot, C. Portet, J. Chmiola, P.-L. Taberna, Y. Gogotsi, P. Simon, *J. Am. Chem. Soc.* **2008**, *130*, 2730.
[103] C. Young, T. Park, J. W. Yi, J. Kim, M. S. A. Hossain, Y. V. Kaneti, Y. Yamauchi, *ChemSusChem* **2018**, *11*, 3546.
[104] W. Raza, F. Ali, N. Raza, Y. Luo, K.-H. Kim, J. Yang, S. Kumar, A. Mehmood, E. E. Kwon, *Nano Energy* **2018**, *52*, 441.
[105] A. M. Abioye, F. N. Ani, *Renewable Sustainable Energy Rev.* **2015**, *52*, 1282.
[106] S. Jung, Y. Myung, B. N. Kim, I. G. Kim, I.-K. You, T. Kim, *Sci. Rep.* **2018**, *8*, 1915.
[107] Y.-P. Gao, Z.-B. Zhai, K.-J. Huang, Y.-Y. Zhang, *New J. Chem.* **2017**, *41*, 11456.
[108] J. Deng, M. Li, Y. Wang, *Green Chem.* **2016**, *18*, 4824.
[109] H. Haykırı-Açma, *Energy Convers. Manage.* **2003**, *44*, 155.
[110] A. Jain, R. Balasubramanian, M. P. Srinivasan, *Chem. Eng. J.* **2016**, *283*, 789.
[111] F. Barzegar, A. Bello, D. Momodu, M. J. Madito, J. Dangbegnon, N. Manyala, *J. Power Sources* **2016**, *309*, 245.
[112] Y. Liu, J. Chen, B. Cui, P. Yin, C. Zhang, *C J. Carbon Res.* **2018**, *4*, 53.
[113] L. Zhu, F. Shen, R. L. Smith, L. Yan, L. Li, X. Qi, *Chem. Eng. J.* **2017**, *316*, 770.
[114] W. Liu, J. Mei, G. Liu, Q. Kou, T. Yi, S. Xiao, *ACS Sustainable Chem. Eng.* **2018**, *6*, 11595.
[115] X.-L. Su, M.-Y. Cheng, L. Fu, J.-H. Yang, X.-C. Zheng, X.-X. Guan, *J. Power Sources* **2017**, *362*, 27.
[116] C.-C. Hu, C.-C. Wang, F.-C. Wu, R.-L. Tseng, *Electrochim. Acta* **2007**, *52*, 2498.
[117] Z. Li, L. Zhang, B. S. Amirkhiz, X. Tan, Z. Xu, H. Wang, B. C. Olsen, C. M. B. Holt, D. Mitlin, *Adv. Energy Mater.* **2012**, *2*, 431.
[118] C. K. Ranaweera, P. K. Kahol, M. Ghimire, S. R. Mishra, R. K. Gupta, *J. Carbon Res.* **2017**, *3*, 25.
[119] W. Qian, F. Sun, Y. Xu, L. Qiu, C. Liu, S. Wang, F. Yan, *Energy Environ. Sci.* **2014**, *7*, 379.
[120] B. Duan, X. Gao, X. Yao, Y. Fang, L. Huang, J. Zhou, L. Zhang, *Nano Energy* **2016**, *27*, 482.
[121] M. D. Stoller, R. S. Ruoff, *Energy Environ. Sci.* **2010**, *3*, 1294.
[122] C. Wu, S. Yang, J. Cai, Q. Zhang, Y. Zhu, K. Zhang, *ACS Appl. Mater. Interfaces* **2016**, *8*, 15288.
[123] W. Wei, X. Cui, W. Chen, D. G. Ivey, *Chem. Soc. Rev.* **2011**, *40*, 1697.
[124] M. Toupin, T. Brousse, D. Bélanger, *Chem. Mater.* **2004**, *16*, 3184.
[125] D. Bélanger, T. Brousse, J. W. Long, *Electrochem. Soc. Interface* **2008**, *17*, 49.
[126] M. Yang, D. S. Kim, S. B. Hong, J.-W. Sim, J. Kim, S.-S. Kim, B. G. Choi, *Langmuir* **2017**, *33*, 5140.
[127] C. Wang, Y. Xiong, H. Wang, Q. Sun, *J. Colloid Interface Sci.* **2018**, *528*, 349.
[128] T. Ouyang, K. Cheng, F. Yang, L. Zhou, K. Zhu, K. Ye, G. Wang, D. Cao, *J. Mater. Chem. A* **2017**, *5*, 14551.
[129] C. Chen, Y. Zhang, Y. Li, J. Dai, J. Song, Y. Yao, Y. Gong, I. Kierzewski, J. Xie, L. Hu, *Energy Environ. Sci.* **2017**, *10*, 538.
[130] Y. Luan, Y. Huang, L. Wang, M. Li, R. Wang, B. Jiang, *J. Electroanal. Chem.* **2016**, *763*, 90.
[131] C. Chen, X. Hu, Z. Wang, X. Xiong, P. Hu, Y. Liu, Y. Huang, *Carbon* **2014**, *69*, 302.
[132] Y. Zeng, M. Yu, Y. Meng, P. Fang, X. Lu, Y. Tong, *Adv. Energy Mater.* **2016**, *6*, 1601053.
[133] F. Lai, Y.-E. Miao, L. Zuo, H. Lu, Y. Huang, T. Liu, *Small* **2016**, *12*, 3235.
[134] D. Shan, J. Yang, W. Liu, J. Yan, Z. Fan, *J. Mater. Chem. A* **2016**, *4*, 13589.
[135] B. Liu, Y. Liu, H. Chen, M. Yang, H. Li, *ACS Sustainable Chem. Eng.* **2019**, *7*, 3101.
[136] S. Kaipannan, S. Marappan, *Sci. Rep.* **2019**, *9*, 1104.
[137] F. Barzegar, A. Bello, J. K. Dangbegnon, N. Manyala, X. Xia, *Energy Procedia* **2017**, *105*, 4098.
[138] K. Karthikeyan, S. Amaresh, S. N. Lee, X. Sun, V. Aravindan, Y. G. Lee, Y. S. Lee, *ChemSusChem* **2014**, *7*, 1435.
[139] T. Ouyang, K. Cheng, Y. Gao, S. Kong, K. Ye, G. Wang, D. Cao, *J. Mater. Chem. A* **2016**, *4*, 9832.
[140] X. Deng, B. Zhao, L. Zhu, Z. Shao, *Carbon* **2015**, *93*, 48.
[141] A. R. Kamali, D. J. Fray, *Chem. Commun.* **2015**, *51*, 5594.
[142] X. Liu, M. Antonietti, *Carbon* **2014**, *69*, 460.
[143] Y. Tang, T. Chen, S. Yu, Y. Qiao, S. Mu, J. Hu, F. Gao, *J. Mater. Chem. A* **2015**, *3*, 12913.
[144] Y. Tang, T. Chen, S. Yu, *Chem. Commun.* **2015**, *51*, 9018.
[145] T. Chen, Y. Tang, Y. Qiao, Z. Liu, W. Guo, J. Song, S. Mu, S. Yu, Y. Zhao, F. Gao, *Sci. Rep.* **2016**, *6*, 23289.
[146] L. Wang, B. Gao, C. Peng, X. Peng, J. Fu, P. K. Chu, K. Huo, *Nanoscale* **2015**, *7*, 13840.
[147] Q. Wang, Y. Zhang, H. Jiang, C. Meng, *J. Colloid Interface Sci.* **2019**, *534*, 142.
[148] K. Chaitra, R. T. Vinny, P. Sivaraman, N. Reddy, C. Hu, K. Venkatesh, C. S. Vivek, N. Nagaraju, N. Kathyayini, *J. Energy Chem.* **2017**, *26*, 56.
[149] K. Chaitra, N. Nagaraju, K. Nagaraju, *Mater. Chem. Phys.* **2015**, *164*, 98.
[150] G. Qu, S. Jia, H. Wang, F. Cao, L. Li, C. Qing, D. Sun, B. Wang, Y. Tang, J. Wang, *ACS Appl. Mater. Interfaces* **2016**, *8*, 20822.
[151] W. Wang, J. Qi, Y. Sui, Y. He, Q. Meng, F. Wei, Y. Jin, *J. Nanosci. Nanotechnol.* **2018**, *18*, 5600.
[152] S. Liu, L. Wang, C. Zheng, Q. Chen, M. Feng, Y. Yu, *ACS Sustainable Chem. Eng.* **2017**, *5*, 9903.
[153] K. Chaitra, R. Narendra, K. Venkatesh, N. Nagaraju, N. Kathyayini, *J. Power Sources* **2017**, *356*, 212.
[154] S. E. M. Pourhosseini, O. Norouzi, P. Salimi, H. R. Naderi, *ACS Sustainable Chem. Eng.* **2018**, *6*, 4746.
[155] P. Sennu, V. Aravindan, Y.-S. Lee, *J. Power Sources* **2016**, *306*, 248.
[156] M. Yu, Y. Han, Y. Li, J. Li, L. Wang, *Appl. Surf. Sci.* **2019**, *463*, 1001.
[157] K. Fang, J. Chen, X. Zhou, C. Mei, Q. Tian, J. Xu, C.-P. Wong, *Electrochim. Acta* **2018**, *261*, 198.
[158] S. Yu, X. Zhu, G. Lou, Y. Wu, K. Xu, Y. Zhang, L. Zhang, E. Zhu, H. Chen, Z. Shen, B. Bao, S. Fu, *Mater. Des.* **2018**, *149*, 184.
[159] M. Huang, F. Li, F. Dong, Y. X. Zhang, L. L. Zhang, *J. Mater. Chem. A* **2015**, *3*, 21380.
[160] L. L. Zhang, X. Zhao, M. D. Stoller, Y. Zhu, H. Ji, S. Murali, Y. Wu, S. Perales, B. Clevenger, R. S. Ruoff, *Nano Lett.* **2012**, *12*, 1806.
[161] B. Liu, M. Yang, H. Chen, Y. Liu, D. Yang, H. Li, *J. Power Sources* **2018**, *397*, 1 – 10.

Manuscript received: July 10, 2019
Accepted manuscript online: July 16, 2019
Version of record online: August 23, 2019